

Computational Analysis of Flow Regulatory Mechanism in Artificial Kidney



**By
Tuba Yaqoob**

**School of Chemical and Materials Engineering
National University of Sciences and Technology**

2020

Computational Analysis of Flow Regulatory Mechanism in Artificial Kidney



Names: Tuba Yaqoob

Reg.No:275247

This thesis is submitted as a partial fulfillment of the requirements for the degree of

MS in Process Systems Engineering

Supervisor Name: Dr. Muhammad Ahsan

**School of Chemical and Materials Engineering
National University of Sciences and Technology,**

H-12 Islamabad, Pakistan

September, 2020



THESIS ACCEPTANCE CERTIFICATE

Certified that final copy of MS thesis written by Ms **Tuba Yaqoob** (Registration No 00000275247), of School of Chemical & Materials Engineering (SCME) has been vetted by undersigned, found complete in all respects as per NUST Statues/Regulations, is free of plagiarism, errors, and mistakes and is accepted as partial fulfillment for award of MS degree. It is further certified that necessary amendments as pointed out by GEC members of the scholar have also been incorporated in the said thesis.

Signature: _____

Name of Supervisor: **Dr Muhammad Ahsan**

Date: _____

Signature (HOD): _____

Date: _____

Signature (Dean/Principal): _____

Date: _____



Form TH-1

National University of Sciences & Technology (NUST)
MASTER'S THESIS WORK
Formulation of Guidance and Examination Committee

Name: **Tuba Yaqoob**NUST Regn No: **00000275247**Department: **SCME**Specialization: **Process Systems Engineering**Credit Hour Completed: **(21) 24**CGPA: **3.93**

Course Work Completed

S/No	Code	Title	Core/Elective	CH	Grade
1	PSE-801	Process Systems Theory	Core	03	A
2	PSE-852	Process Modelling and Simulation	Core	03	A
3	PSE-823	Advanced Process Dynamics and Control	Core	03	A
4	PSE-802	Optimization and Decision Analysis	Core	03	A
5	CSE-801	Computation Fluid Dynamics (CFD)	Elective	03	A
6	EME-902	Numerical Methods for CHE (Chemical Engineering)	Elective	03	A
7	TEE-810	Advanced Process Energy Analysis & Optimization	Elective	03	B+
8	RM-898	Research Methodology	Additional	2	Q

Date 16/7/2019

Student's Signature

Thesis Committee

1. Name: **Dr. Arshad Hussain (Supervisor)**

Department: Chemical Engineering

Signature:

2. Name: **Dr. Muhammad Ahsan**

Department: Chemical Engineering

Signature:

3. Name: **Dr. Iftikhar Ahmad**

Department: Chemical Engineering

Signature:

Date: 16/7/2019

Signature of Head of Department:

APPROVALDate: 16/7/2019
Dean/Principal**Distribution**

1x copy to Exam Branch, HQ NUST

1x copy to PGP Dte, HQ NUST

1x copy to Exam branch, respective institute

School of Chemical and Materials Engineering (SCME) Sector H-12, Islamabad



Form: TH-04

National University of Sciences & Technology (NUST)

MASTER'S THESIS WORK

We hereby recommend that the dissertation prepared under our supervision by

Regn No & Name: 00000275247 Tuba Yaqoob

Title: Computational Analysis of Flow Regulatory Mechanism in Artificial Kidney.

Presented on: 03 Sep 2020 at: 1200 hrs in SCME on MS Teams

Be accepted in partial fulfillment of the requirements for the award of Master of Science degree in Process System Engineering.

Guidance & Examination Committee Members

Name: Dr Iftikhar Ahmad

Signature: 

Name: Dr Sarah Farrukh

Signature: 

Supervisor's Name: Dr Muhammad Ahsan

Signature: 

Dated: 08.09.2020


Head of Department

Date 07/9/2020


Dean/Principal

Date 10/9/2020

School of Chemical & Materials Engineering (SCME)

Dedication

Dedicated to my Beloved Parents, Brother and family.

ACKNOWLEDGEMENTS

All acclaim and eminence be to "ALLAH" a definitive creator of this universe, who endowed us with the ability to comprehend and made us curious to investigate this entire universe. Infinite greetings upon the leader of this universe and hereafter "HOLY PROPHET HAZRAT MUHAMMAD (P.B.U.H)": the wellspring of beneficial information and blessings for whole humankind and Uma.

I wish to express my heartiest and sincerest gratitude to Dr. Muhammad Ahsan, for his guidance, inspiration, constructive suggestion, devotion and close supervision throughout the entire period of the work. I am grateful for the support provided by him during my entire program. It was a great privilege and honor working under his supervision. It is an experience I am going to cherish for the rest of my life.

I would also like to thank the advisory committee members of this project – Dr. Iftikhar Ahmad and Dr. Sarah Farrukh for their valuable and insightful comments on this project.

Special thanks to Engr. Ahmad Yaqoob, for financial, moral and educational support throughout this program.

Abstract

There is an enormous need in the health welfare sector to manufacture inexpensive dialyzer membranes with minimum dialysis duration. In order to optimize the dialysis cost and duration, an in-depth analysis of the effect of dialyzer design and process parameters on toxins (ranging from small to large size molecules) clearance rate is required. The efficiency of this transport phenomena depends on the hollow fiber geometry, membrane characteristics and operating variables. It is difficult to translate the in vivo transfer process with in vitro experiments as it involves high cost to produce various designs and membranes for dialyzer.

Mathematical analysis and enhanced computational power of computers can translate the transport phenomena occurring inside the dialyzer while minimizing the development cost. In the past 30 years numerous mathematical models have been proposed to mimic the transport phenomena occurring in vivo. The models have been simulated through different software including MATLAB[®], ANSYS Fluent[®] and COMSOL Multiphysics[®]. In vitro analysis to optimize the membrane characteristics and module geometry have also been performed side by side. However, due to little communication between the in vitro and in silico research there is no efficient tool for the wet lab workers that enables them to rigorously determine the effect of membrane properties and other process parameters on clearance efficiency of dialyzer module. This void hinders to develop a membrane module that efficiently mimics the function of human kidney. To the best of authors' knowledge, COMSOL Inc. has developed an application that enable to study the effect of few membrane properties and design parameters on module clearance efficiency but it does not mimic the transport phenomena associated with dialyzers merely because of the simplicity of the mathematical model. Nevertheless, it inspires towards the development of a better application that could reduce the cost of R&D needed to optimize membrane properties and module design.

In first part of this study, a steady-state microscopic balance was developed to mimic the convective and diffusive transport of low molecular weight (LMW) solutes i.e. urea and glucose and middle molecular weight (MMW) solutes i.e. endothelin and β 2-Microglobulin inside the dialyzer. The aim of computational analysis performed with these model equations is to figure out those factors that play vital role in enhancing the dialyzer clearance. Tortuous Pore Diffusion Model (TPDM) was used to mimic the transport of solute inside the porous medium and convection-diffusion equations were used to establish the mass transfer in blood

and dialysate compartment. In the second part, development of a user-friendly stand-alone application is described thoroughly.

Keywords: artificial kidney; hemodialysis; membrane; hollow fiber dialyzer, CFD

CONTENTS

Dedication	i
Acknowledgements	ii
Abstract	iii
CONTENTS	v
LIST OF FIGURES	viii
LIST OF TABLES	xi
List of Abbreviations	xii
CHAPTER 1: INTRODUCTION	1-8
1.1 Motivation for computational analysis of artificial kidney	1
1.2 The Kidney	1
1.3 Kidney Failure	2
1.3.1 Urea	2
1.3.2 Glucose	3
1.3.3 Endothelin	3
1.3.4 β 2-Microglobulin	3
1.3.5 Complement Factor D	3
1.3.6 Albumin	3
1.4 Hemodialysis	4
1.4.1 Working principle	4
1.4.2 Blood Circulation Path	5
1.4.3 Dialysate Circulation Path	6
1.4.4 Dialyzer (Artificial kidney)	7
CHAPTER 2: LITERATURE REVIEW	9-16
2.1 Literature Review	9
2.2 Objectives	15
2.3 Outline of forthcoming chapters	16
CHAPTER 3: DEVELOPMENT OF MATHEMATICAL MODEL	17-27
3.1 Development of Model	17
3.2 Mathematical Modeling	18
3.3 Governing Equations-Blood side ($i=B$)	19
3.4 Transfer of solutes across the multilayer membrane ($j=skin,middle,bulk$)	20
3.5 Tortuous Pore Diffusion Model (TPDM) for membrane coefficient	21

3.6 Governing Equations- Dialysate side ($i=D$)	22
3.3 Computational Method	23
3.4 Validation	25
CHAPTER 4: RESULTS AND DISCUSSION	28-38
4.1 Results and Discussion	28
4.2 Effect of operating conditions on clearance efficiency	28
4.3 Effect of module geometry on solute clearances	32
4.3.1 Effect of fiber length on clearance rate	32
4.3.2 Effect of fiber radius on clearance rate	34
4.3.3 Effect of fiber aspect ratio	35
4.3.4 Effect of skin layer pore size on clearance rate	36
CHAPTER 5: DEVELOPMENT OF STAND-ALONE APPLICATION	39-55
5.1 Motivation for building a stand-alone application	39
5.2 Introduction to Application Builder	39
5.3 Switching the COMSOL Environment	39
5.4 Development of Forms	40
5.4.1 Main Form	42
5.4.2 Input Form	44
5.4.3 Description form	45
5.4.4 Results form	46
5.4.5 Info form	46
5.4.6 Geodraw form	47
5.5 Development of Methods	48
5.5.1 p_report Method	48
5.5.2 p_input_changed Method	49
5.5.3 p_init_application Method	49
5.5.4 p_solve_and_plot Method	50
5.5.5 p_create_result_table Method	50
5.6 Development of the File Menu and Ribbon tab	51
5.6.1 Reset to Default item	51
5.6.2 Update item	52
5.6.3 Compute item	52
5.6.4 Report item	53

5.6.5 Open PDF Documentation item	53
5.7 Compiler	54
5.8 Comparison of Stand-alone Application with COMSOL Application	54
CHAPTER 5: CONCLUSION AND FUTURE RECOMMENDATIONS	56-57
6.1 Conclusion	56
6.2 Recommendations	57
References	58

LIST OF FIGURES

Figure 1. Blood filtration system in Human Kidney	2
Figure 2. Blood circulation path in hemodialysis machine	5
Figure 3. Dialysate circulation path	6
Figure 4. Crimps of hollow fibers and shape of dialyzer (FX100)	8
Figure 5. Kolff's initial design of tubular dialyzer	10
Figure 6. Pore diffusion model (PDM) vs Tortuous pore diffusion model (TPDM)	13
Figure 7. Framework of the geometry of dialyzer module (lower panel) with its model developed in this work (upper panel)	18
Figure 8. Simulation work-flow in COMSOL Multiphysics 5.4	25
Figure 9. Axisymmetric concentration contour of urea at both blood and dialysate side and across the membrane	26
Figure 10. Urea clearance rate for in-silico and in-vitro cases at varying blood flow rate with constant dialysate flow rate ($Q_D=500\text{ml/min}$)	27
Figure 11. Model predicted (solid lines) vs in vivo and in silico (symbols) solute clearances plotted against varying blood flow rate at $Q_D=500\text{ml/min}$	29
Figure 12. Model predicted (solid lines) vs in vivo and in silico (symbols) solute clearances plotted against varying blood flow rate at $Q_D=500\text{ml/min}$	29
Figure 13. Model predicted (solid lines) vs in vivo and in silico (symbols) solute clearances plotted against varying dialysate flow rate at $Q_B=400\text{ml/min}$	31
Figure 14. Model predicted (solid lines) vs in vivo and in silico (symbols) solute clearances plotted against varying Dialysate flow rate at $Q_B=400\text{ml/min}$	31
Figure 15. Clearance rate of low molecular weight solutes (urea, glucose) plotted against varying length of the dialyzer at $Q_B=300\text{ml/min}$ and $Q_D=500\text{ml/min}$	33
Figure 16. Clearance rate of high molecular weight solutes plotted against varying length of the dialyzer at $Q_B=300\text{ml/min}$ and $Q_D=500\text{ml/min}$	33
Figure 17. Clearance rate of low molecular weight solutes plotted against varying radius of the dialyzer at $Q_B=300\text{ml/min}$ and $Q_D=500\text{ml/min}$	34

Figure 18. Clearance rate of high molecular weight solutes plotted against varying radius of the dialyzer at $Q_B=300\text{ml/min}$ and $Q_D=500\text{ml/min}$	35
Figure 19. Dimensionless urea clearance rate plotted with varying fiber aspect ratio	36
Figure 20. Effect of pore diameter on clearance rate of urea and glucose	37
Figure 21. Effect of pore diameter on clearance rate of large molecular weight (LMW) molecules	37
Figure 22. Switching from Model Builder to Application Builder	40
Figure 23. Application Builder environment of COMSOL Multiphysics	40
Figure 24. Forms created to build the application	41
Figure 25. Form Objects available in COMSOL Application Builder to develop Forms	42
Figure 26. Form Objects used in Left-half of the Main form	43
Figure 27. Form Objects used in Right-half of the Main form	44
Figure 28. The Input form developed with Form Objects	44
Figure 29. Description form developed with Form Object	45
Figure 30. Result form developed with Form Objects	46
Figure 31. Info form developed with Form Objects	46
Figure 32. Geodraw developed with Form Object	47
Figure 33. New Method nodes created to build a series of actions during application run	47
Figure 34. Report nodes created in model building environment to set the format and features of report	48
Figure 35. if-else loop used to generate the report of results in application	48
Figure 36. Code written in the p_input_changed node	48
Figure 37. Code written in the p_init_application node	49
Figure 38. Code written in the p_solve_and_plot node	49
Figure 39. Code written in the p_create_result_table node	50
Figure 40. Step wise development of sections and sub-sections of File Menu and Ribbon Tab	51
Figure 41. Command sequence included in Reset to Default Item	51
Figure 42. Command sequence included in Update item	52
Figure 43. Command sequence included in Compute item	52

Figure 44. Command for report generation	53
Figure 45. Command to see associated PDF file	53
Figure 46. Compiler to create a stand-alone application	53
Figure 47. Comsol application window (Left side) vs Stand alone application window (Right side)	54

LIST OF TABLES

Table 1 Molecules that were examined in the computational analysis with their molecular weight and diameter	32
Table 2 Comprehensive dataset of model parameters used for model predictions	36
Table 3 Comparison of this model results with literature data	39
Table 4 Maximum percentage difference of this model with literature data at varying blood flow rate	42
Table 5 Maximum percentage difference of this model with literature data at varying dialysate flow rate	44
Table 6 Maximum percentage difference of this model with literature data at varying dialyzer fiber length	46
Table 7 Maximum percentage difference of this model with literature data at a varying radius of dialyzer fiber	47
Table 8 Maximum percentage difference of this model with literature data at varying aspect ratio of dialyzer fiber	48
Table 9 Maximum percentage difference of this model with literature data at varying pore diameter of dialyzer fiber	50
Table 10 Property Data set for COMSOL application vs Stand-alone Application	55

List of Abbreviations

$c_{s,i}$	molar concentration of the s-th solute in the i-th compartment [mol/litre]
Cl_s	Clearance rate of the j-th solute [ml/min]
$D_{e,s}$	Diffusivity of s-th solute in the i-th compartment [m^2/s]
d_i	diameter of the i-th compartment [mm]
F	friction coefficient
K_s	overall mass transfer coefficient of s-th solute [m/s]
$k_{s,i}$	mass transfer coefficient of s-th solute in the i-th compartment [m/s]
$k_{s,mj}$	mass transfer coefficient of s-th solute in the j-th membrane layer
L	length of the fiber [mm]
N	total number of fibers [-]
$N_{Sh,i}$	Sherwood number in the i-th compartment [-]
$N_{Re,i}$	Reynold number in the i-th compartment [-]
p	ratio of solute radius to the pore radius
Q_B	blood flow rate in the blood compartment [ml/min]
Q_D	dialysate flow rate in the dialysate compartment [ml/min]
r_1	inner radius of the fiber [mm]
r_2	radius up to the outer layer of the fiber [mm]
r_3	radius of the concentric permeate channel [mm]
S_D	steric hinderance factor at pore inlet
u_i	axial velocity in the i-th compartment [m/s]
v_i	radial velocity in the i-th compartment [m/s]
z	axial co-ordinate [m]

Subscript and superscript

B	blood
D	dialysate
e	effective
i	i-th compartment (B,m,D)

in inlet
 j j-th membrane layer (skin,middle,bulk)
 m membrane

Greek symbols

δ_j thickness of the j-th membrane layer
[mm]
 ε_{mj} membrane j-th layer porosity
[-]
 μ_i fluid viscosity in the i-th compartment [kg/ms]
 ρ_i fluid density in the i-th compartment

CHAPTER 1

INTRODUCTION

1.1 Motivation for computational analysis of artificial kidney

The major applications of membrane technology in medical field are kidney dialysis (hemodialysis), oxygenation of blood and control diffusion of drugs in blood. Financial measures show that manufacturing cost of dialyzer (Artificial Kidney) is about US\$15 and they are usually disposed off after one session. Consequently, the trade of this small device is generating a revenue of approximately US\$2 billion [1-3].

Dialyzers, used in hemodialysis machines, are equipped with synthetic polymeric membranes and work as an artificial kidney. Since Pakistan is importing these cellulosic membranes, hemodialysis is an expensive treatment for our patients. Membrane research group (MEMAR) at NUST is working on the indigenous development of cellulose acetate membranes. The improvement in performance of the membrane dialyzer requires better understanding of flow regulatory mechanism of artificial kidney. Several mathematical models have been developed to study urea clearance, protein rejection and kinetics of minerals present in the blood. However, a wholesome approach to simulate the flow regulatory mechanism of artificial kidney yet to be developed to design an efficient membrane dialyzer.

1.2 The Kidney

Every human body has two bean-shaped organs known as kidneys. These kidneys are placed on the left and right side in the retroperitoneal space. These organs actually function like a blood filtration plants for our body. Kidneys, other than filtrating urea and toxins, regulate the urinary system, acid - base balance and arterial hypotension. So, these two small organs play a vital role in sustaining healthy body. There are three major processes performed inside the kidney:

1. **Glomerular filtration:** Water and toxins smaller than protein are forced through the glomerular capillaries into the Bowman's capsule and Renal tubule.
2. **Tubular Reabsorption:** Some important minerals like glucose, amino acids and water are reabsorbed back into the blood through peritubular capillaries.
3. **Tubular Secretion:** Important ions like H^+ and K^+ and drugs are removed from peritubular capillary.

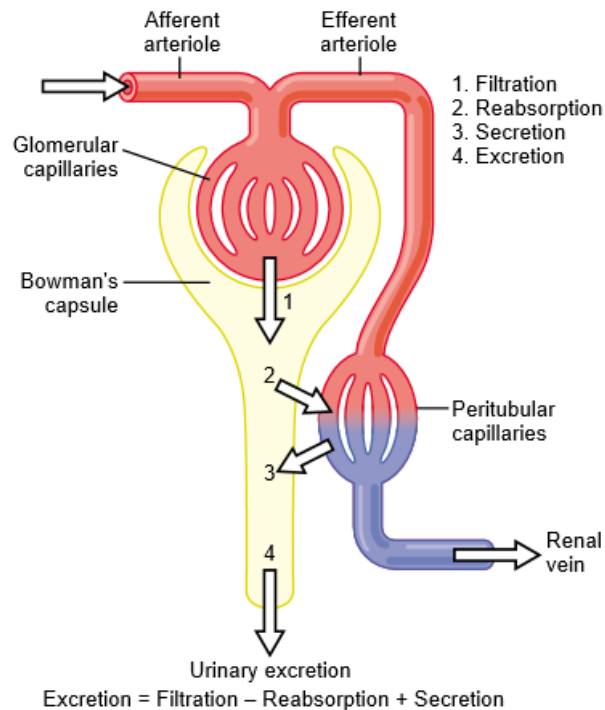


Figure 1. Blood filtration system in Human Kidney [4]

1.3 Kidney Failure

Kidney is actually a complex bundle of semi-permeable porous hollow fibers. When these fibers lose their ability to filter the water and toxins from blood streams, the situation is generally described as kidney failure. In more sophisticated terms, the function of kidney is measured by its Glomerular Filtration Rate (GFR). If GFR is observed below 15% the patient is diagnosed with End Stage Renal Failure (ESRF) [5]. ESRF patients observe an increase in creatinine level [6]. Due to reduction in GFR, the body fluid levels are elevated. pH level decreases and Urea, glucose, endothelin, β 2-macroglobulin, and complement factor D observe abnormal levels [6,7]. These molecules can be described as follows:

1.3.1 Urea Urea (Carbamide, $\text{CO}(\text{NH}_2)_2$) removes nitrogen-based components from blood and excrete these harmful substances through urine. Uremia is a disease observed in ESRF patients due to elevated level of Blood Urea Nitrogen (BUN) [8]. Uremia introduces several other imbalances in the body that ultimately leads to the following conditions:

- ◆ Anorexia
- ◆ Lethargy
- ◆ Fatigue

- ◆ Nausea
- ◆ Bone Pain
- ◆ Breath shortness
- ◆ Seizures to mental acuity
- ◆ Coma

1.3.2 Glucose Although glucose play a vital role in our metabolism but its increase in blood raise the blood sugar level and ultimately leads to diabetes. If the kidney does not filter excess amount of glucose from blood the kidney patient will become diabetic as well, and dialysis will be the ultimate solution [9].

1.3.3 Endothelin Kidney patients also suffer from hypertension due to the imbalance of endothelin. Actually, these molecules are involved in growth of smooth blood vessels but they can hinder the blood flow and cause hypertension if kidney does not function properly. In kidney failure Endothelin molecules are raised in the blood [10].

1.3.4 β 2- Microglobulin It maintains and control the peptide binding. Elevated level of β 2- Microglobulin agglomerate as amyloid fibers. One of the reasons of joint pain is accumulation of amyloid fiber in joint interstices. In kidney failure excess amount of these molecules starts accumulating in blood and ultimately cause joint pain [11].

1.3.5 Complement Factor D Obesity is caused by elevation of this molecule in blood. The reason of its increase is not clear but in kidney patients Complement Factor D is not filtered from blood stream [12].

Albumin is a protein which we have to keep in blood during dialysis. These molecules play a vital role in muscles growth.

1.3.6 Albumin In blood plasma the most important protein is Albumin. It is responsible for transportation of hormones as well as fatty acids. Albumins are also binding water and ions with other substances. The oncotic pressure (blood osmotic pressure due to proteins) is regulated by Albumin. We need to minimize the loss of Albumin during dialysis [13,14].

Before 1960, the ESRF was a fatal condition but today three major treatments are available for such patients [15].

- **Kidney Transplant** Organ transplant is the best and permanent solution for ESRF but it is a surgical procedure with a high cost. Secondly, it is very difficult to find a living potential donor.

- **Peritoneal Dialysis** The word peritoneal is derived from peritoneum- a thin membrane surrounding the abdominal and pelvic region. The blood is filtered inside the body using this natural membrane. This treatment is less convenient because everyday patients need 4-6 hrs. for this procedure.
- **Hemodialysis** In this treatment patient blood is pumped to an external circuit equipped with a dialyzer - a small filter like a shell and tube heat exchanger. The session takes 4 hrs. and usually happens 3 times per week. Its more convenient for the patients.

1.4 Hemodialysis

Hemodialysis machine consist of a blood circulation path, a dialysate circulation system and a dialyzer. The hollow fiber inside the dialyzer separates two streams- blood stream and dialysate stream. The blood circuit consist of:

- A vascular access device
- Blood pumps (1-2)
- Pressure – air leakage detectors

The dialysate flow system components are:

- Dialysate fluid containers (pure water and concentrated solution)
- Dialysate heating system
- Ultrafiltration control system
- Dialysis fluid pumps

The dialysate circulation, pumping system, leakage and pressures are continuously monitored. The hollow fiber tubules inside the dialyzer play a vital role in this whole process because these membrane fibers are responsible to purify blood toxins, urea and excess water and also responsible for retaining the important blood cells and proteins in blood stream.

1.4.1 Working principle

The phenomena behind the whole process of purification is diffusion of small size solute molecules, across the porous semi-permeable hollow fibers, due to concentration gradient - more specifically chemical potential gradient. This difference in chemical potential elevate the value of Gibb's free energy of blood side molecules, and enable them to move from high concentration point towards the low concentration point. Hemodialysis machines works on counter current flow system. The dialysate and blood streams flow in parallel and opposite direction.

1.4.2 Blood Circulation Path

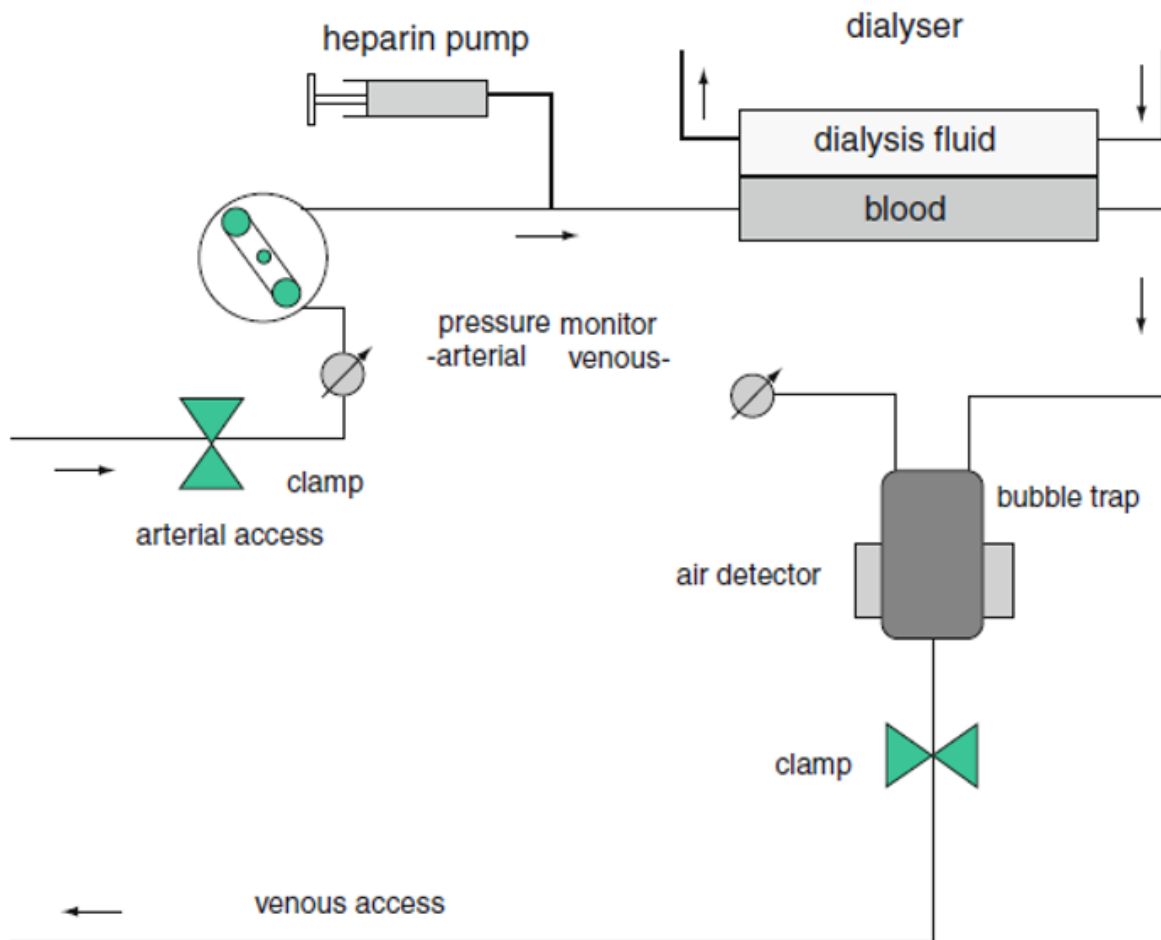


Figure 2. Blood circulation path in hemodialysis machine [16]

The blood from the body is pumped to the hollow fiber dialyzer. This is done by connecting the arterial and venous blood lines to the lower and upper dialyzer ports respectively. Clean or less contaminated blood from the dialyzer pass through an air detector (air trap) to ensure the de-aeration of blood. After this process, the blood is recirculated to the patient's body. Air bubbles are detected by ultrasound devices. If any air is detected in the blood circulation path the machine is immediately stopped. The tubing set used to connect arterial and venous system to the dialyzer ports is made of polyvinylchloride and polycarbonate. Although, the dialyzer filter is used in one session, for one patient only, some residues may exist in the tubing, which can cause serious infections and diseases to the other patients. Therefore, sterilization of the blood circulation path is an extremely important part of this procedure. Either steam or ethylene oxide can serve the purpose. Steam is usually preferred over ethylene oxide as it may form anti-body and can give allergic reactions.

1.4.3 Dialysate Circulation Path

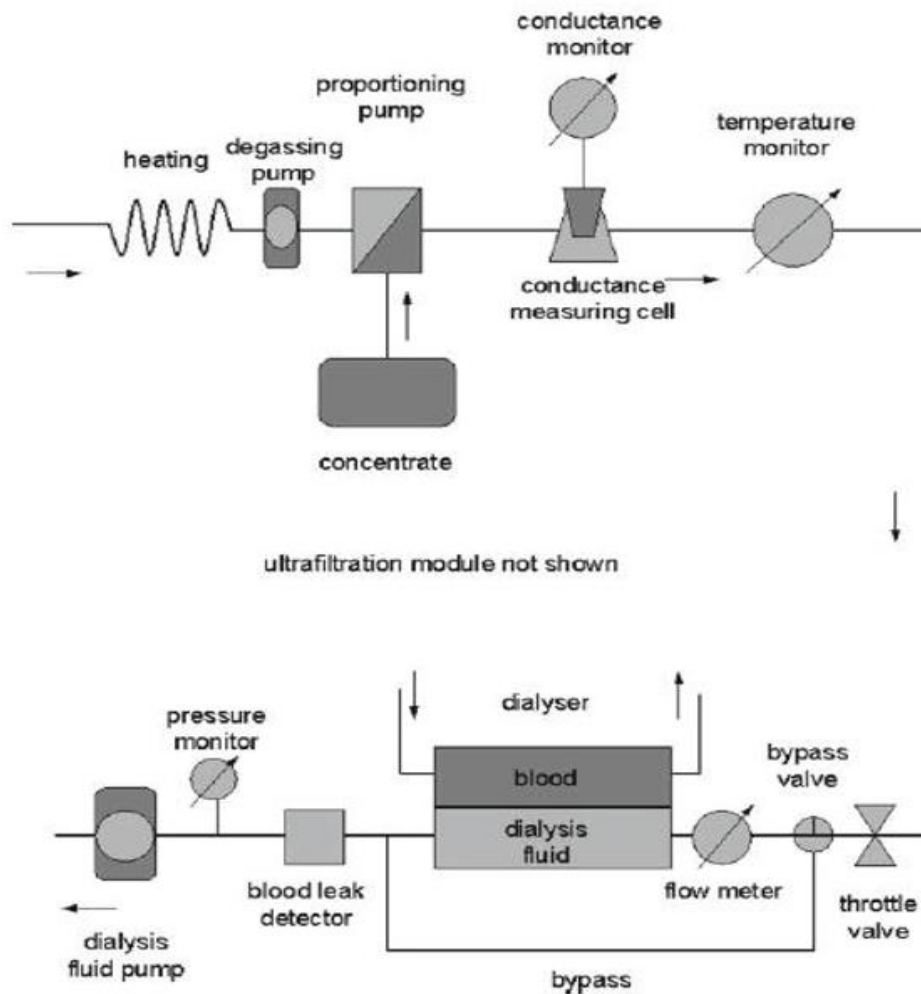


Figure 3. Dialysate circulation path [16]

Dialysate is prepared by highly purified water and concentrated electrolyte solution. A small water purification plant is usually installed within the dialysis center. The plant has water softening system, activated carbon filter, sedimentation unit and reverse osmosis unit. The formation of air or gas bubbles on the surface of hollow fiber is avoided through continuous degassing of the dialysate. The clearance rate is reduced, if degassing is not done properly. To maintain the composition of dialysate solution, the dialysate conductance and temperature is continuously monitored. In this way, hypo and hyper thermic situations are avoided.

1.4.4 Dialyzer (Artificial kidney)

Dialyzer actually plays the role of artificial kidney for End Stage Renal Failure (ESRF) patient. This is the most vital part of the hemodialysis machine because the blood plasma is filtered

inside the hollow fibers of this dialyzer. The dialyzer flow pattern is analogous to shell and tube heat exchanger where blood and dialysate flow in a countercurrent manner. Since the membrane is porous and semipermeable some of the solute molecules pass through and other are retained in blood stream. The morphological characteristics of membrane decide the diffusion and rejection of molecules. Some important characteristics that determine the efficiency of dialyzer are:

- Clearance rate
- Sieving coefficient
- Ultrafiltration coefficient
- Membrane Permeability

The capillary tubules or hollow fibers are confined inside a small cylindrical housing. A variety of dialyzer, available in the market, are classified on the basis of flux and other design parameters. The classification of dialyzer on the basis of fiber material is as follows:

- Cellulosic fiber dialyzer
- Synthetic fiber dialyzer

Among these two categories the cellulosic fiber dialyzers are less expensive. Cuprophan is a famous cellulosic membrane with several hydroxyl groups. These functional groups activate undesired complements in the blood. A better version of Cuprophan is Hemophan because it esterifies most of the hydroxyl groups. Despite of all these improvements the cellulosic fibers can initiate coagulation in the blood.

Due to the above-mentioned drawbacks of cellulosic fibers the manufacturers moved toward the synthetic materials. These synthetic materials are basically polymers - used to manufacture hollow fibers. Some famous polymers are:

- Polyamide
- Polysulfone
- Polyethersulfone
- Polymethylmethacrylate (PMMA)
- Polyarylethersulfone/Polyamide

Although synthetic fibers do not completely eradicate the formation of undesirable residues, but lower the activation of this process to a great extent. The clearance efficiency of synthetic fibers is also greater than cellulosic fibers due to larger pores and thick wall. Although large pores increase clearance rate but they also allow essential molecules like Albumin to diffuse in

dialysate. So, the target of manufacturer is to produce a membrane which provides maximum removal of toxins with maximum rejection of Albumin.



Figure 4. Crimps of hollow fibers and shape of dialyzer (FX100) [17]

CHAPTER 2

LITERATURE REVIEW

2.1 Literature Review

The commercial use of membrane separation technique was started with the progression of Cerein dialyzer (an Italian Company that produces medical devices and RO systems). Application of membrane technology in the medical field is equal to the overall membrane usage in the industry (membrane distillation, pervaporization, liquid-liquid extraction). If we look at the monetary worth of membrane based medical devices, their demand and worth is considerably high. Although membrane applications are found in commercial industry as well as in health care sector, but we hardly found connection between these two areas of membrane application. As a result, both kind of membrane manufacturers have separate research journals, committees and conferences. So, there exist no collaboration between these two domains [15].

A study of 2015 by Kifayat Ullah and co-workers reported that in Pakistani society occurrence of different events of kidney failure is more than hundred in a million [18]. There is enormous need in the health welfare sector to manufacture amendable and inexpensive dialyzer membranes in order to enhance the attributes of blood dialysis machines. There are several brands of dialyzer membranes fabricated by various corporations, with varying strength and weaknesses. Yet, we are facing challenges on minimizing the dialysis duration along with making them recyclable, bio-compatible and economical by technological alterations in bio-tech.

Conard et al. presented the historical background about the development of extracorporeal therapies (hemodialysis and hemofiltration) for ESRD patients. It was 1981 when a Scottish physical chemist, named Graham, did the separation of large size particles from smaller ones by applying the concept of diffusion using a porous skin. For the first time in history, Willem Kolff clinically used dialysis to save the life of an ESRD patient [19]. In the beginning Kolf 's dialysis machines, shown in the **Figure 5**, were applicable only for patients who had been facing acute kidney failure due to some injury or toxicity.

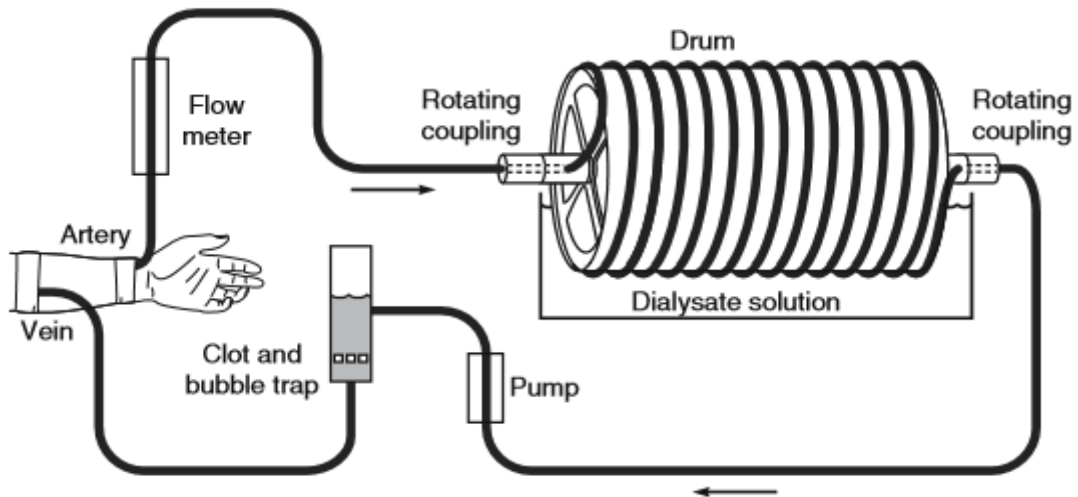


Figure 5. Kolff's initial design of tubular dialyzer [20]

For such patients only few sessions of dialysis were required. Till the beginning of 1960s this therapy was only used for emergency cases. The reason for rare use of hemodialysis therapy was the incompatible design of hemodialysis machine for chronic kidney patients as they need 2-3 dialysis sessions in a week for years, and it was not possible with initial designs. Later in 1960s, the design of dialyzer was improved to make it compatible for ESRD patients. An important improvement in the design was the use of plastic shunt that could be constantly fixed to patient's Arterio-Venous blood lines to provide an approach to blood circulatory system. This improvement introduced by Scribner et al. [21] permitted to link the hemodialysis machine, excluding the requirement of surgical procedure, to the patient's arterio-venous system. The initial design of Kolf's machine, comprised of tubular dialyzer, needed many liters of blood, to make sure that the extracorporeal circuit is well primed. This was the main drawback in this design. In 1950s, Kolf suggested the spiral shape of tubes, and in the beginning of 1960, spiral design was the first, industrially manufactured, discardable dialyzer. Still the blood needed to flush the tubes of dialyzer was unreasonable and during 1960s, further modification leads us to the plate and frame and hollow fiber dialyzers. It was 1975, when in the US the market of dialyzers was divided into spiral, hollow fiber and plate and frame designs as 65 %, 20 % and 15 %, respectively. The coil(spiral) shape design became obsolete in the coming ten years, and only 1/3 plate and frame with 2/3 hollow fiber systems were available. Now-a-days, hollow fiber is the only manufactured design of the dialyzer [15].

Zydney AL, for the first time, modeled the phenomena of bulk or convective transfer across the hollow fibers and established the fact that convective transport across membrane play a

vital role in enhancing the clearance efficiency of high-flux hemodialysis. The model equations for blood dialysate compartments and membrane were developed with both diffusive and convective transport [22].

Jaffrin MY suggested an empirical correlation for the calculation of total clearance including the effect of both diffusive and convective transport. The correlation is:

" $K = K_D + 0.43Q_f + 8.3 \times 10^{-3}Q_f$ ". In this correlation Q_f is ultrafiltration flow rate. Author has discussed three different models, published earlier, to calculate the clearance rate by using sieving coefficient and outlet toxins concentration. The results obtained by this correlation were in good agreement with in-vitro results of other authors [23].

Akcahuseyin E et al. established the difference between the conventional hemodialysis and "Continuous Arterio-Venous Hemodiafiltration (CAVHD)" transfer process. In conventional procedure only diffusion is the dominant phenomena with zero ultrafiltration, whereas in CAVHD ultrafiltration flows are prominent. Therefore, the overall mass transfer coefficient in these two procedures cannot be identical. However, at low values of ultrafiltration flow the mass transfer coefficient of CAVHD becomes equal to that of conventional hemodialysis [24].

β 2-Microglobulin saturation in blood can cause amyloidosis (amyloid accumulation in cells and organs). Raj DS investigated the kinetics of β 2-Microglobulin during two therapeutic modalities i.e Conventional Hemodialysis (CHD) and Nocturnal Hemodialysis (NHD). This was an in-vivo study carried out over ESRF patients. Results show that Urea and Creatinine removal was not so different in both therapies but β 2-Microglobulin clearance was significantly higher in NHD compared with CHD. Author establish from this research that Amyloidosis can be delayed for a longer period in ESRF patients by applying NHD as it decreases the pre-dialysis concentration of β 2-Microglobulin in blood [25].

Legallais C developed a theoretical model to study the impact of module design parameters, membrane characteristics and process parameters on the module clearance efficiency. The model has incorporated the phenomena of concentration polarization and variation of mass transfer coefficient with flow rate, and change in water flux along the module length. By replacing saline and plasma with blood, the model estimates within 10% and 20% of in-vivo results, respectively [26].

Coli et al. developed a mathematical model for body fluids and solutes transport. For fluids transport, a 3-compartment model was proposed including plasma, interstitial space and

intracellular space. On the other hand, the solute transfer was explained with a 2-dimensional model. In vivo clinical data of the patients was used to validate the simulation profiles. The results show variation in solutes (Urea, Sodium, Potassium, Chloride and Bicarbonate) concentration, and change in ultrafiltration profile with time. These results were in good agreement with patient's data [27].

The phenomena of hemodiafiltration is combination of diffusion and ultrafiltration flux across the membrane. The small size low molecular weight (LMW) molecules i.e urea and creatinine are transported by simple diffusion whereas middle size molecules are transported by ultrafiltration flux [28]. The mathematical equations used to calculate the solute flux and ultrafiltration flux are:

$$J_v = L_p(P_B - P_D - \Delta\Pi)$$

$$J_s = K_o(C_B - C_D) + J_v\gamma(f_B C_B + f_D C_D)$$

These model equations are discussed in a number of research articles with little difference in symbols [26-30]. J_s and J_v are solute and ultrafiltration fluxes respectively, γ is sieving coefficient, which has value ranging from 0 to 1. The sieving coefficient is taken 1 for urea and lesser than 1 for large size particles. L_p is hydraulic permeability, which is multiplied with difference of osmotic ($P_B - P_D$) and oncotic pressure $\Delta\pi$. C_B and C_D represent the local concentration of blood and dialysate compartment.

Galach M et al. reported the comparison of Waniewski, Legallais and Jaffrin models. All these models are one dimensional and use different assumptions to determine the mass transfer coefficient across the membrane [28]. The model presented by Legallais has taken into account the individual mass transfer coefficient i.e at blood – membrane interphase and dialysate – membrane interphase and inside the membrane [26,28]. Waniewski on the other hand has lumped up the overall mass transfer coefficient into membrane permeability [28-29]. While Jaffrin developed an empirical correlation – as mentioned earlier that shows the dependence of transmittance coefficient on ultrafiltration flow rates [28,30].

Conard et al. did Finite Element Analysis (FEA) of the hollow fiber hexagonal shape compartmental geometry. The convection-diffusion equation for mass transport and continuity equation with Navier-Stokes equation for momentum transport were applied [31]. The effect of concentration polarization on osmotic pressure and boundary layer was incorporated by Merrill equation [32]. The porous media was modeled with Brinkman equation. Blood was

considered a non-Newtonian fluid and Carreau-Gambarodo model was used to explain the non-Newtonian behavior of blood [33].

Galach M et al. developed a virtual patient model to explain the physiological phenomena during dialysis. This model helps in selection of dialysis treatment for a patient. The author has shown that how the blood glucose level, and volume changes with time, during hemodialysis and peritoneal dialysis [34].

Yamamoto K et al. proposed that “Tortuous Capillary Pore Diffusion Model (TCPDM)” gives better estimation of diffusive permeability and water flux as compare to simple “Pore Diffusion Model (PDM)”. Tortuosity makes the length of diffusional path longer than the straight right-angle displacement [35].

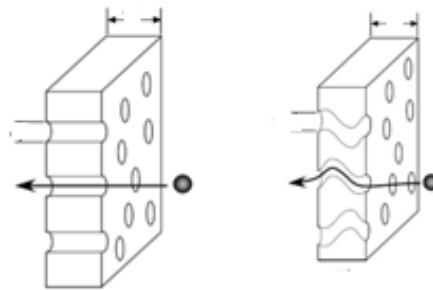


Figure 6. Pore diffusion model (PDM) vs Tortuous pore diffusion model (TPDM) [35]

Azar et al. reported that the urea reduction ratio and dialyzer clearance rate is elevated by enhancing the dialysate flow. This was an in-vivo study, performed on 138 dialysis patients, and statistical analysis of the collected data proved this fact [36].

Olson JC proposed a new idea in hemodialysis traditional treatment by introducing the design of portable hemodialysis system. Simulink was used to design the system model. This model work on several inputs, including dialyzer geometry, therapy time and blood flow rate. The proposed model was validated against in vitro experimental results obtained from porcine blood, and other published data of hemodialysis patients [5].

Lu J. et al. did the computational analysis of flow through parallel paths of porous channels. Navier Stokes equation and Kedem-Katchalsky (K-K) model is simulated to develop the velocity field and concentration distribution profile [37].

Shihamul Islam with coworkers studied commercially available dialyzer membrane called Polyflux 210H manufactured by Gambro Dialysatoren- a German company. Some process parameters and design parameters were provided by company [38]. The morphological aspects

of membrane were determined by Field emission Scanning Electron microscopy (FESEM). The author applied PDM with COMSOL Multiphysics 4.3 to simulate the mathematical model of this membrane [16]. The author does not incorporate tortuosity factor in his model, that is an essential characteristic of the asymmetric synthetic polymeric membrane. Although tortuosity does not impact the clearance of small size molecules, but has a huge impact on the clearance of middle size and big molecules. The big size particles face more hinderance by the zig-zag transfer path than the straight channel. Such a channel helps in rejecting Albumin molecules.

Annan K worked on the design of blood and dialysate inlet outlet headers and studied their impact on the uniformity of flow. The flow profiles were developed through mathematical modeling. The results show that the design of collars, for dialysate solution inlet, introduce non-uniform flow, and ultimately affect the solute exchange through the membrane [39].

Daveport A has discussed the evolution of design of dialyzer from cellulosic coil drum to hollow fiber smart shape of synthetic capillaries and phenomena of modern dialyzer in detail [40]. Ding W et al. developed 3D geometry of dialyzer including the housing, blood and dialysate inlets and outlets and hollow fibers. They compared the velocity and concentration profile of blood and dialysate compartments with magnetic resonance imaging (MRI) results. COMSOL Multiphysics software was used to develop the geometry and simulation of dialyzer. Simulation results have shown that clearance rate of toxins increases by increasing blood and dialysate flow [41].

Zhang Q et al. worked on the preparation of a new polymeric material that gives better clearance of urea with maximum Albumin rejection. He proposed that Polyvinylidene fluoride (PVDF) material fibers worked better than commercially available Fresenius polysulfone (F60S). The results show that protein rejection was 82.3% with water permeability of $108.2 \text{ Lh}^{-1}\text{m}^{-2}$. The ultrafiltration coefficient was found to be 62.6 ml/h/mmHg [42].

The models presented earlier considered a fixed inlet concentration of solute, and not flexible to update the concentration with time. Ravagli E et al. updated the mathematical model of hollow fiber by connecting it with blood pool model. As a result, the model is capable of updating change in the blood concentration with time [43].

Mimouni Z studied the change in blood viscosity with shear rate. If the shear rate is below 10^{-2} , blood flow in capillaries follow the non-Newtonian fluid behavior, and above this value the behavior is Newtonian. The author has discussed two models to explain the nature of blood

flow in capillaries. The two models are Quemada model and Carreau – Gambaruto model. The results obtained with these two models are compared with experimental curve. There was a point of inflection in the curve that was explained by the phenomena of rouleaux [33].

Donato D et al. use the concept of non-dimensionalization of mathematical model and made a set of dimensionless numbers. Out of these numbers the author discussed those which impact dimensionless clearance. The simulated results are very close to the experimental data. The author has shown the impact of fiber aspect ratio, membrane pressure modulus and module packing density on the overall clearance rate of different solutes. COMSOL Multiphysics Finite element method (FEM) code is used in this paper [44].

Sangeetha et al. did the comparison between clearance rate of straight and wavy structure of hollow fibers. The results show that wavy fibers significantly enhance the clearance efficiency of dialyzer, but the mechanical strength of fiber reduces by increasing the waviness. So, one has to optimize the design between mechanical strength and clearance efficiency [45].

2.2 Problem Statement

The previous studies have presented a simplified description of solute transport across the membrane by assuming uniform convective flux that permits to solve the model equations analytically. However, the analytical solution provides the results only at inlet and outlet of the hollow fibers. Therefore, in current study a CFD model is solved with Finite Element Method that provides solution on a large number of points present in the computational domain. Some mathematical models established the solute transport from blood to the dialysate side and across the membrane with an overall mass transfer coefficient. The use of overall mass transfer coefficient without considering the tortuosity and porosity of porous media introduce difference between the in vitro and in silico clearance rates. To fill this void, TPDM is used in this study that incorporates the effect of membrane tortuosity and porosity to give better estimation of overall mass transfer coefficient.

2.3 Objectives

Most of the existing research is based on 2D or 3D mathematical models, simulated with the help of COMSOL Multiphysics software, but none has provided any application for the users to study the impact of change in process variables and design parameters on clearance rate of the dialyzer. Although COMSOL Inc. has introduced the idea of such an application, but the application does not represent the transport of different solutes through membrane [46]. So, the

objective of this study is not only to develop a mathematical model of the dialyzer, but also to build a stand-alone application that enable the users to run the mathematical model with desired parameters, and study the impact of change on the clearance rate of toxins.

Polyflux H210 membrane characteristics were used to simulate the mathematical model. This is a multilayered membrane with different porosity levels. The results of simulated model are compared with Islam et al. and manufacturer data.

So, the main objectives of this study are:

1. To develop a model that enable us to predict the clearance rate of dialyzer at different design parameters and process variables.
2. To optimize the clearance efficiency of the dialyzer.
3. To develop a standalone user-friendly application to see performance of the dialyzer under varying conditions.
4. To facilitate medical doctors and researchers to understand performance of dialyzer under varying conditions.

2.4 Outline of forthcoming chapters

In chapter 3, the development of mathematical model of dialyzer including blood side, membrane and dialysate side is discussed in detail. It also includes the computational methods used in COMSOL Multiphysics. Chapter 4 discuss the results obtained from the simulated model and Chapter 5 gives conclusion and recommendations. Chapter 6 is based on the development of stand-alone application.

CHAPTER 3

DEVELOPMENT OF MATHEMATICAL MODEL

3.1 Development of Model

A framework of hollow fiber module is presented in Figure 7. A collection of about 12000 hollow fibers is enclosed in an external shell. Blood passes through the cavity of hollow fibers and dialysate, an aqueous solution of electrolytes, circulates counter-currently over the fibers. The transfer of molecules between the blood and dialysate compartment and across the semi-permeable membrane is governed by diffusion and convection. In the presented model, the fibers are assumed to be uniformly spaced, organized in a hexagonal order, and interstice among the adjacent annuli are neglected. It is essential to mention that uneven spacing among fibers would results in lowering of overall mass transfer coefficient on the shell side, leading to a decline of dialyzer efficiency due to non-uniform distribution of dialysate streams therein. However, the increase of dialyzer flow rate in certain regions of the shell side partially counter balance the impact of non-uniform distribution in other areas. The solutes considered to study the transport phenomena inside the dialyzer are shown in Table 1.

Table 1 Molecules that were examined in the computational analysis with their molecular weight [47] and diameter [48]

Molecule	Molecular Mass (Da)	Radius (nm)
Urea	60	0.24
Glucose	180	0.5
Endothelin	4282.8	1.30
β 2-Microglobulin	11800	1.94
Complement Factor D	24000	2.56
Albumin	66000	3.9

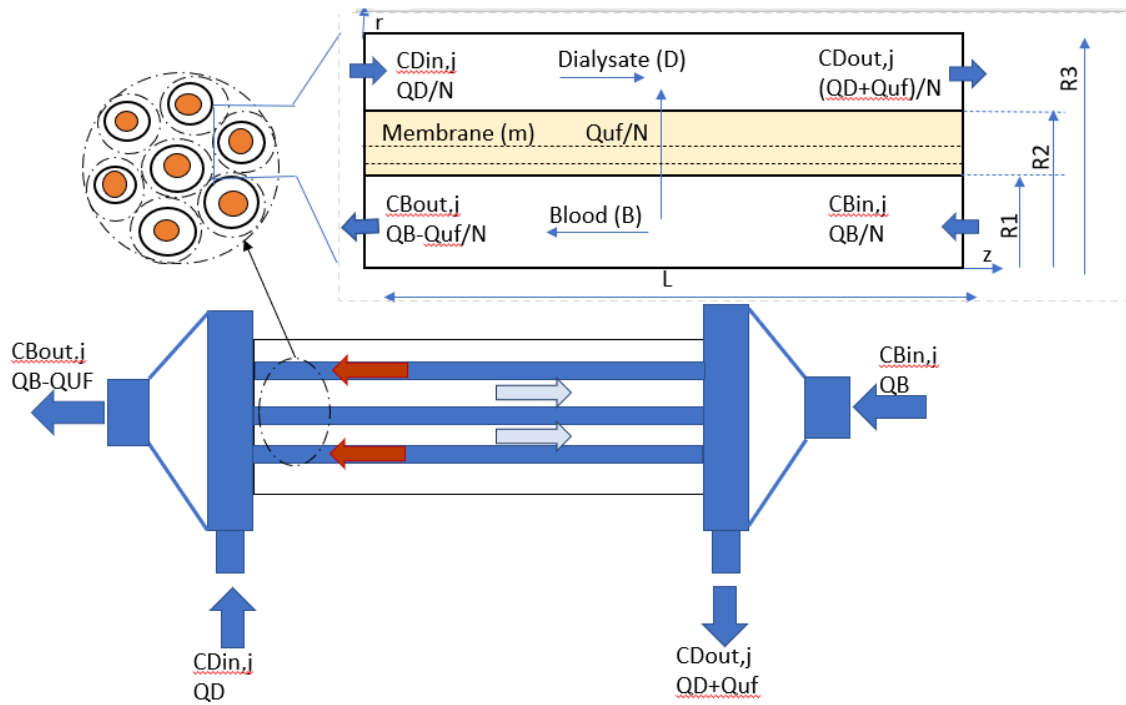


Figure 7. Framework of the geometry of dialyzer module (lower panel) with its model developed in this work (upper panel)

3.2 Mathematical Modeling

Following assumptions are made regarding the module framework shown in Figure 7.

- i. Steady-state and laminar flow condition prevail on both blood and dialysate side
- ii. Isothermal conditions ($T = 37^{\circ}\text{C}$)
- iii. Axial symmetry
- iv. Two-dimensional transport of mass and momentum considered
- v. Blood and dialysate are taken as an incompressible and Newtonian fluid
- vi. Gravitational effects are neglected
- vii. The velocity profiles on both blood and dialysate side are portrayed with the Navier-Stokes equations [49]
- viii. A three-layer isotropic semi-permeable membrane with a skin, middle and bulk layer was considered [50]
- ix. Solute transport through the membrane was described with Tortuous Pore Diffusion Model (TPDM) [35]

- x. Sieving coefficient remains constant
- xi. High dilution of solutes

The governing equations and boundary conditions which describe momentum and mass transport in both blood and dialysate compartments and across the membrane are as follows:

3.3 Governing equations -Blood side (i=B)

A cylindrical co-ordinate system with two dimensions (r,z) is considered, where dialyzer length (i.e. $0 \leq z \leq L$) is taken along the z-direction and radius (i.e. $0 \leq r \leq r_3$) is taken along r-direction. The steady fully developed flow of blood can be described with continuity equation (Eq. 1) and Navier Stokes equation (Eq. 2-3). Equation 2 and 3 are written for radial and axial velocity components, respectively.

$$\frac{1}{r} \frac{\partial}{\partial r} (rv_i) + \frac{\partial u_i}{\partial z} = 0 \quad (1)$$

$$r) \quad v_B \frac{\partial v_B}{\partial r} + u_B \frac{\partial v_B}{\partial z} = \frac{-1}{\rho_B} \frac{\partial P_B}{\partial r} + \frac{\mu_B}{\rho_B} \left[\frac{1}{r} \frac{\partial}{\partial r} \left(r \frac{\partial v_B}{\partial r} \right) - \frac{v_B}{r^2} + \frac{\partial^2 v_B}{\partial z^2} \right] \quad (2)$$

$$z) \quad v_B \frac{\partial u_B}{\partial r} + u_B \frac{\partial u_B}{\partial z} = \frac{-1}{\rho_B} \frac{\partial P_B}{\partial z} + \frac{\mu_B}{\rho_B} \left[\frac{1}{r} \frac{\partial}{\partial r} \left(r \frac{\partial u_B}{\partial r} \right) + \frac{\partial^2 u_B}{\partial z^2} \right] \quad (3)$$

At $z=0$ and $0 < r < r_1$, a fully developed inlet velocity profile for N number of fibers obtained by solving Eq. 1 to 3 is:

$$v_B(r) = 0 \quad \text{and} \quad u_B(r) = \frac{2Q_B}{N\pi r_1^2} \left[1 - \left(\frac{r}{r_1} \right)^2 \right] \quad (4)$$

In equation 4, Q_B (ml/min) is blood flow rate in each of the hollow fiber and πr_1^2 is cross-sectional area of the fiber. Equation 5 and 6 represent that the axial velocity is maximum at $r=0$ and no slip conditions prevail at the walls of the membrane, respectively.

$$v_B = \frac{\partial u_B}{\partial r} = 0 \quad \text{at} \quad r = 0; \quad 0 \leq z \leq L \quad (5)$$

$$v_B = u_B = 0 \quad (6)$$

The convection-diffusion equation that governs the mass transfer of solutes s present in the blood is:

$$u_B \frac{\partial c_s}{\partial z} + v_B \frac{\partial c_s}{\partial r} = D_s \left(\frac{\partial^2 c_s}{\partial r^2} + \frac{1}{r} \frac{\partial c_s}{\partial r} + \frac{\partial^2 c_s}{\partial z^2} \right) \quad (7)$$

Here, $c_s (kg/m^3)$ and $D_s (m^2/s)$ are the concentration and the bulk diffusivity of solutes s , respectively. The boundary conditions to solve equation 7 are:

$$\forall z \text{ at } r = 0 \text{ and } r = r_1 \quad c_{s,i}(r, 0) = c_{s,in}$$

and

$$\frac{\partial c_{s,i}}{\partial r} = 0 \text{ where } i = B$$

3.4 Transfer of solutes across the Multilayer membrane (j=skin, middle, bulk)

During dialysis process, the thin porous membrane selectively allows the low molecular weight solutes to diffuse into a low concentration region. The flux of solutes is proportional to concentration gradient. The general equation to calculate the solute flux across the membrane is:

$$J_s = K_s (C_{s,B} - C_{s,D}) \quad (8)$$

Here, $J_s (m^3/m^2s)$ and $K_s (m/s)$ presents the solute s flux across the membrane and membrane overall mass transfer coefficient, respectively. $C_{s,B}$ and $C_{s,D}$ are concentration of solute s in the blood and dialysate compartment. Considering the boundary layers on each side of the membrane the interfacial resistances can be taken in series as:

$$\frac{1}{K_s} = \frac{1}{k_{s,B}} + \frac{1}{k_{s,mj}} + \frac{1}{k_{s,D}} \quad (9)$$

Here, $\frac{1}{k_{s,B}}$ and $\frac{1}{k_{s,D}}$ account for the blood and dialysate side boundary layer resistences, respectively. $\frac{1}{k_{s,mj}}$ presents the resistance offered by three consecutive layers of membrane. In order to calculate the mass transfer coefficients of blood and dialysate sides, i.e. $k_{s,B} (m/s)$ and $k_{s,D} (m/s)$, following a generic correlation was used [21]. For annulus, the hydraulic diameter was used for the calculation of the Reynold number.

$$N_{Sh,i} = 1.62 \left(N_{Re,i} N_{Sc,i} \frac{d_i}{z} \right)^{1/3} \quad \text{where } i = B, D \quad (10)$$

and

$$N_{Re,i} = \frac{u_i d_i \rho_i}{\mu_i} ; S_{C_i} = \frac{\mu_i}{\rho_i D_i} \quad (11)$$

Here, $N_{Sh,i}$, $N_{Re,i}$ and $N_{Sc,i}$ are presenting Sherwood number, Reynold number and Schmidt number, respectively.

3.5 Tortuous pore diffusion model (TPDM) for membrane transfer coefficient

The mass transfer coefficient of solute s in j th layer of the membrane $k_{s,mj}$ (m/s) is determined by TPDM. The transfer of solutes s within the membrane is hindered by the tortuosity and porosity of multi-layer membrane. Actually, the pores do not present a straight path for molecules, and the curved shape of the path is quantified by its tortuosity. Tortuous pore diffusion model (TPDM) used to account for all the hinderance causing factors of the porous medium is presented below.

$$k_{s,mj} = \frac{D_{es,j}}{\delta_j} \quad (42)$$

$$D_{es,j} = \left(\frac{D_{s,i} \epsilon_{mj}}{\tau} \right) F(p) H_D \quad (13)$$

where,
$$F(p) = \frac{1 - 2.1050p + 2.0865p^3 - 1.7068p^5 + 0.72603p^6}{1 - 0.75857p^5} \quad (14)$$

$$p = \frac{R_s}{R_p} \quad (15)$$

$$H_D = (1 - p)^2 \quad (16)$$

The equation (13) presents the Tortuous Pore Diffusion Model (TPDM) used to calculate the effective diffusivity $D_{es,j}$ (m^2/s) of solutes s in the porous medium which is less than the

bulk diffusivity $D_{s,i}(m^2/s)$. Friction coefficient $F(p)$ account for the friction that exist between the pore wall and the solute molecules, and p is the ratio of solute radius R_s to the pore radius R_p . The steric hinderance factor H_D presents the volume fraction available for the solute molecules in the cylindrical pore. Tortuosity τ defined by the ratio of pore length to the membrane thickness and the experimentally determined values of tortuosity were taken from Yamamoto et al. [17]. ϵ_{mj} presents the porosity of j th layer of the membrane and its experimentally determined values were taken from Islam et al [22].

3.6 Governing equations - Dialysate side (i=D)

In hollow fiber dialyzer the fibers were surrounded by a uniform annulus as shown in figure 1. The radius of the annulus r_3 is larger than fiber radius r_1 . The velocity of dialysate is also determined by solving continuity equation (8) and Navier Stokes equation (9,10) with specified boundary conditions of $u_z = 0$ at $r=0$ and $r=r_2$. Here, r_2 is the outer radius of membrane.

$$\frac{1}{r} \frac{\partial}{\partial r}(rv_i) + \frac{\partial u_i}{\partial z} = 0 \quad (17)$$

$$r) \quad v_D \frac{\partial v_D}{\partial r} + u_D \frac{\partial v_D}{\partial z} = \frac{-1}{\rho_D} \frac{\partial P_D}{\partial r} + \frac{\mu_D}{\rho_D} \left[\frac{1}{r} \frac{\partial}{\partial r} \left(r \frac{\partial v_D}{\partial r} \right) - \frac{v_D}{r^2} + \frac{\partial^2 v_D}{\partial z^2} \right] \quad (18)$$

$$z) \quad v_D \frac{\partial u_D}{\partial r} + u_D \frac{\partial u_D}{\partial z} = \frac{-1}{\rho_D} \frac{\partial P_D}{\partial z} + \frac{\mu_D}{\rho_D} \left[\frac{1}{r} \frac{\partial}{\partial r} \left(r \frac{\partial u_D}{\partial r} \right) + \frac{\partial^2 u_D}{\partial z^2} \right] \quad (19)$$

The fully developed axial velocity profile of dialysate is:

$$v_D = \frac{2Q_D}{N\pi \left(\frac{3r_3^4}{4} + \frac{r_2^4}{4} - r_2^2 r_3^2 - r_3^4 \ln \left(\frac{r_3}{r_2} \right) \right)} \left[r^2 - r_2^2 - 2r_3^2 \ln \left(\frac{r}{r_2} \right) \right] \quad (20)$$

Here, $v_D(m/s)$ and Q_D (ml/min) are representing the velocity and volumetric flow rate of dialysate, respectively. The governing equation for dialysate side of solutes s transport can be written similar to the equation (7):

$$u_D \frac{\partial c_s}{\partial z} + v_D \frac{\partial c_s}{\partial r} = D_s \left(\frac{\partial^2 c_s}{\partial r^2} + \frac{1}{r} \frac{\partial c_s}{\partial r} + \frac{\partial^2 c_s}{\partial z^2} \right) \quad (21)$$

After simulating the mathematical model, the efficiency of the dialyzer (artificial kidney) was determined by calculating the clearance rate of toxins. The dialyzer clearance rate is measured by the following equation [22]:

$$Cl_s = \frac{Q_B(c_{s,in} - c_{s,out})}{c_{s,in}} \quad (22)$$

3.7 Computational Method

For numerical integration of the mathematical model, the Finite Element Method was applied with COMSOL Multiphysics 5.4. Free triangular meshing was used to perform the discretization of the computational domain. The maximum and minimum element size was kept 2.1×10^{-4} and 9×10^{-7} , respectively, with a maximum growth rate of 1.3 and a curvature factor of 0.3. Two study nodes were included in the solver configuration, i.e., fully Coupled and Direct. Fully Coupled node combines multi-physics domains, i.e., blood, dialysate, and different membrane layers, while applying the Newton's method damped version. Under Direct node MUMPS (Multifrontal Massively Parallel Sparse) method was chosen to enhance the computational efficiency. This method performs the factorization of linear systems in the form of $Ax=b$, where matrix A is factorized to determine the solution 'x'. By using the literature-reported values of model parameters, as listed in Table 2, steady-state 2D profiles of velocity and solute concentration were determined.

Table 2 Comprehensive dataset of model parameters used for model predictions [16,35]

Parameters	Values	Units
Inner radius of the fiber, r_1	0.10	mm
Radius up to the outer layer, r_2	0.145	mm
Radius of the concentric permeate channel, r_3	.210	mm
Length of the fiber, L	270	mm
Tortuosity, τ	2.27	
Inlet concentration, $c_{s,in}$	1	mol/liter
Inlet blood flow rate, Q_B	300	ml/min
Inlet dialysate flow rate, Q_D	500	ml/min
Total number of fibers, N	12000	
Porosity of skin layer, ε_s	0.1	
Porosity of middle layer, ε_m	0.27	
Porosity of bulk layer, ε_b	0.4	
Average size of skin layer pores, d_s	39.5	nm
Average size of middle layer pores, d_m	450	nm
Average size of bulk layer pores, d_b	20400	nm

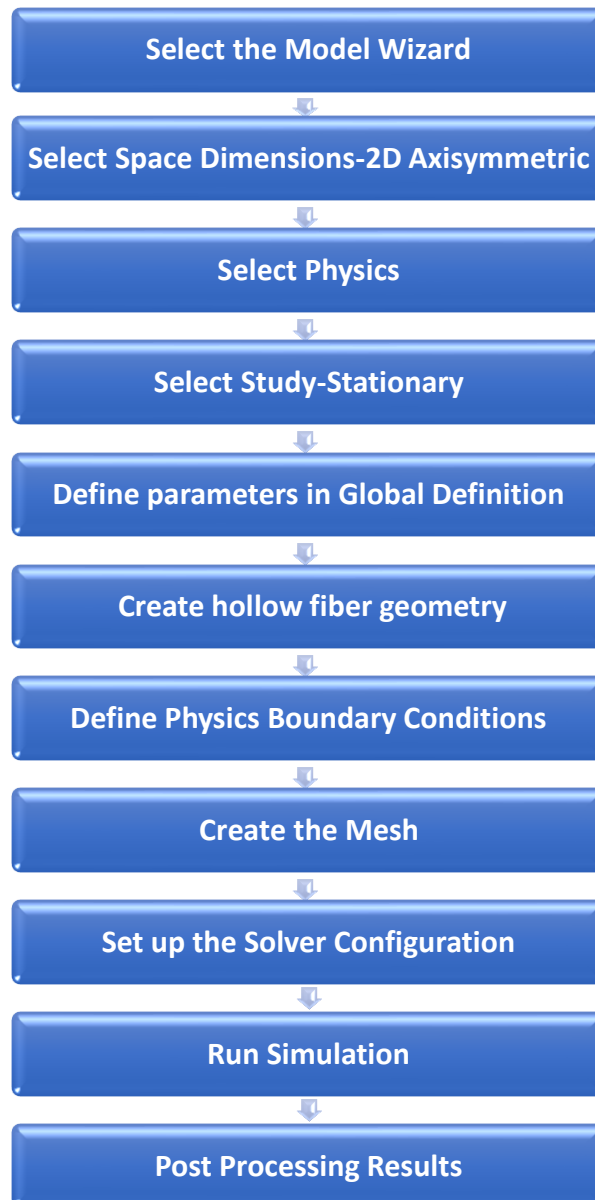


Figure 8. Simulation work-flow in COMSOL Multiphysics 5.4

3.8 Validation

The mathematical model developed was simulated in COMSOL Multiphysics 5.4 with certain inlet, outlet and boundary conditions, by changing different parameters. The concentration contour of urea in blood and dialysate compartment and across the membrane is shown in Figure 9.

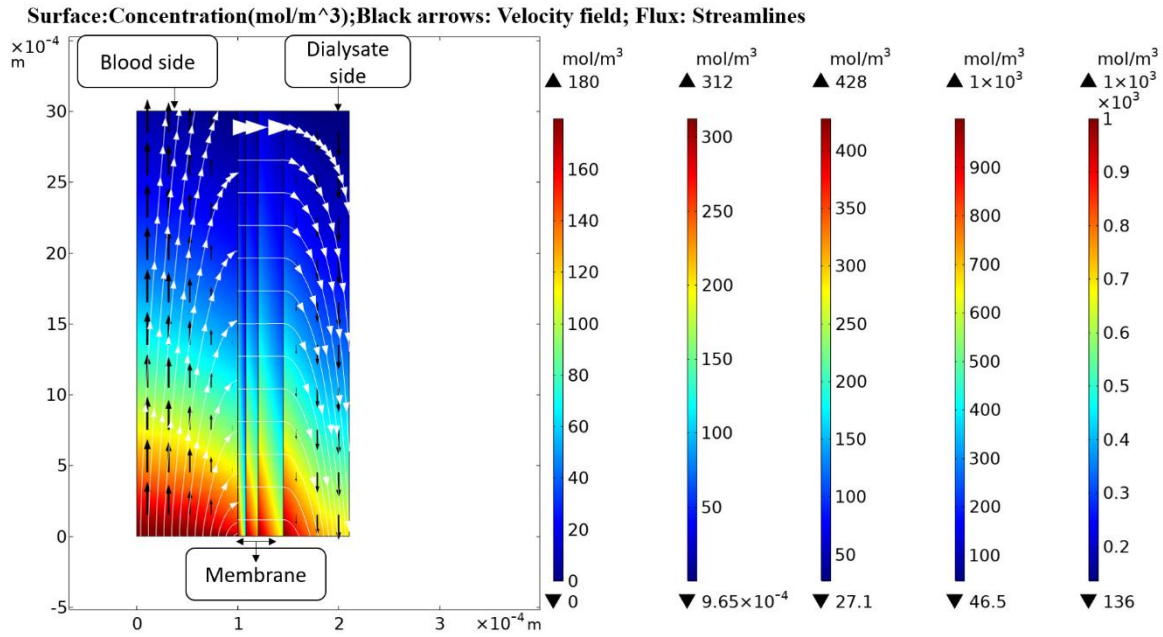


Figure 9. Axisymmetric concentration contour of urea at both blood and dialysate side and across the membrane

In order to validate the proposed mathematical model, the model-predicted urea clearance rate was compared with Islam et al. (in-silico) [16] and experimental data reported in literature [38] at increasing blood flow rates. In Figure 10, the clearance rate of urea is compared with Polyflux 210H data provided by manufacturer [38]. The values of experimental clearance rate, in figure 10, are reported in literature with combined effect of diffusion and ultrafiltration. In table 3, the percentage difference between experimental data and the model predicted values is due to the fact that the ultrafiltration flux across the membrane was not included in the current model. However, the model predicted values for diffusive transport of solute across the membrane are in good agreement with the Islam et al (in silico) results.

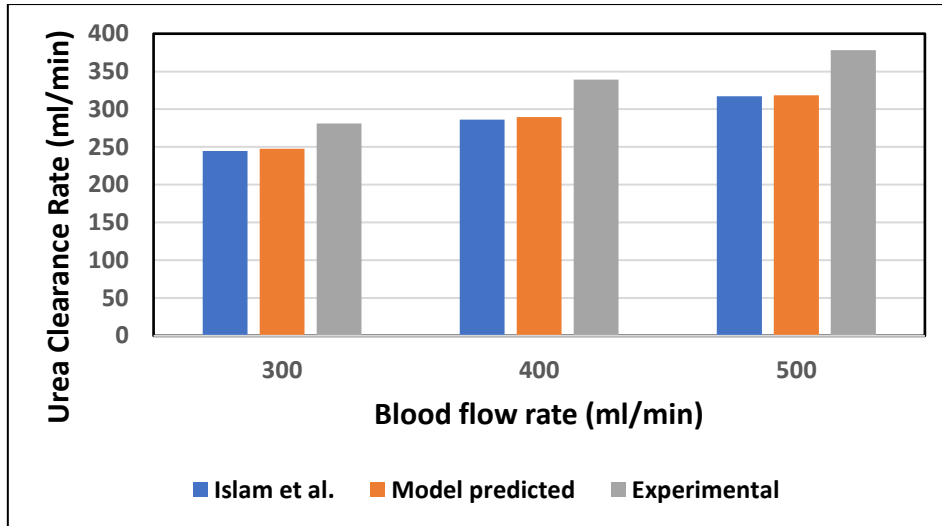


Figure 10. Urea clearance rate for in-silico and in-vitro cases at varying blood flow rate with constant dialysate flow rate ($Q_D=500\text{ml/min}$)

Table 3. Comparison of this model results with literature data [16,38]

Blood flow rate (ml/min)	Model predicted	Islam et al.	Polyflux 210H	Percentage Difference of model predicted and manufacturer data	Percentage Difference of Islam et al. and manufacturer data
300	247.77	244.62	281	11.82	1.28
400	289.52	286.40	339	14.59	1.08
500	318.44	317.04	378	15.75	0.4

CHAPTER 4

RESULTS AND DISCUSSION

4.1 Results and Discussion

The aim of developing this mathematical model was to investigate the impact of module geometry and operating conditions on clearance efficiency and to provide a model that can be simulated at different values of parameters in order to optimize the clearance rate.

4.2 Effect of operating conditions on clearance efficiency

For model parameters, manufacturer data of Polyflux 210H (Gambro Dialysatoren GmbH, Germany, a subsidiary of Baxter International Inc.) was used and predicted clearance rate of different solutes were compared with Islam et al. [16], Theranova 400 MCO AA (Gambro Dialysatoren GmbH, Germany, a subsidiary of Baxter International Inc.), Polyflux 210H [38] and FX CorDiax 80 (Fresenius Medical Care, Bad Homburg, Germany) [52]. The blood flow rate was varied from 300 to 500ml/min keeping dialysate flow rate constant ($Q_D=500\text{ml/min}$). In-silico and in-vivo clearance rates plotted, against varying blood flow rates, were found in good agreement with each other. It is evident from Figure 11 and 12 that the increase in blood flow rate increases the clearance of LMW solutes (urea, glucose) but does not affect the clearance of solutes with high molecular weight. The clearance rate of Albumin is nearly constant. The increase in clearance with blood flow rate can be attributed to rise of concentration difference across the membrane. Transport of solutes is driven by concentration gradient across the membrane. By increasing the blood flow rate, the concentration gradient was increased that ultimately enhance the clearance rate of solutes. On the other hand, the clearance of large size molecules shown in Figure 6 was not affected much due to higher value of steric hinderance H and friction coefficient $F(p)$. Due to high value of steric hinderance H , lesser volume is available for the large size molecules to pass through the cylindrical pore. The effect of steric hindrance H and friction coefficient $F(p)$ was pronounced in Figure 6 while moving from β_2 microglobulin to albumin due to increase in size of molecules.

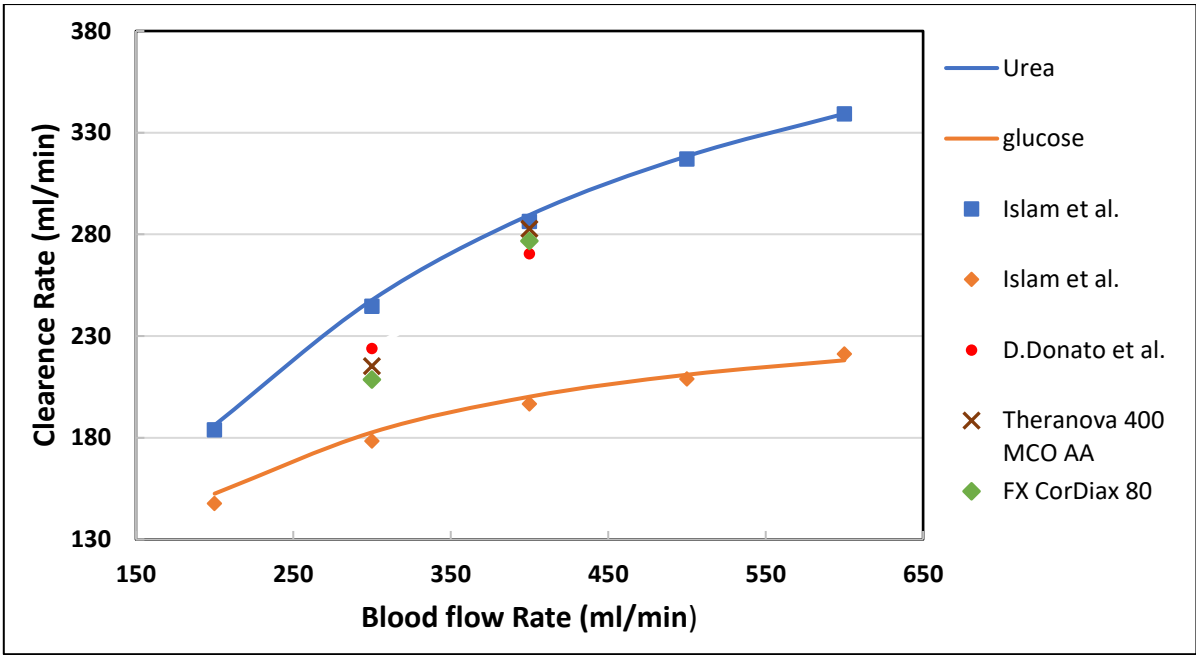


Figure 11. Model predicted (solid lines) vs in vivo and in silico (symbols) solute clearances plotted against varying blood flow rate at $Q_D=500\text{ml/min}$

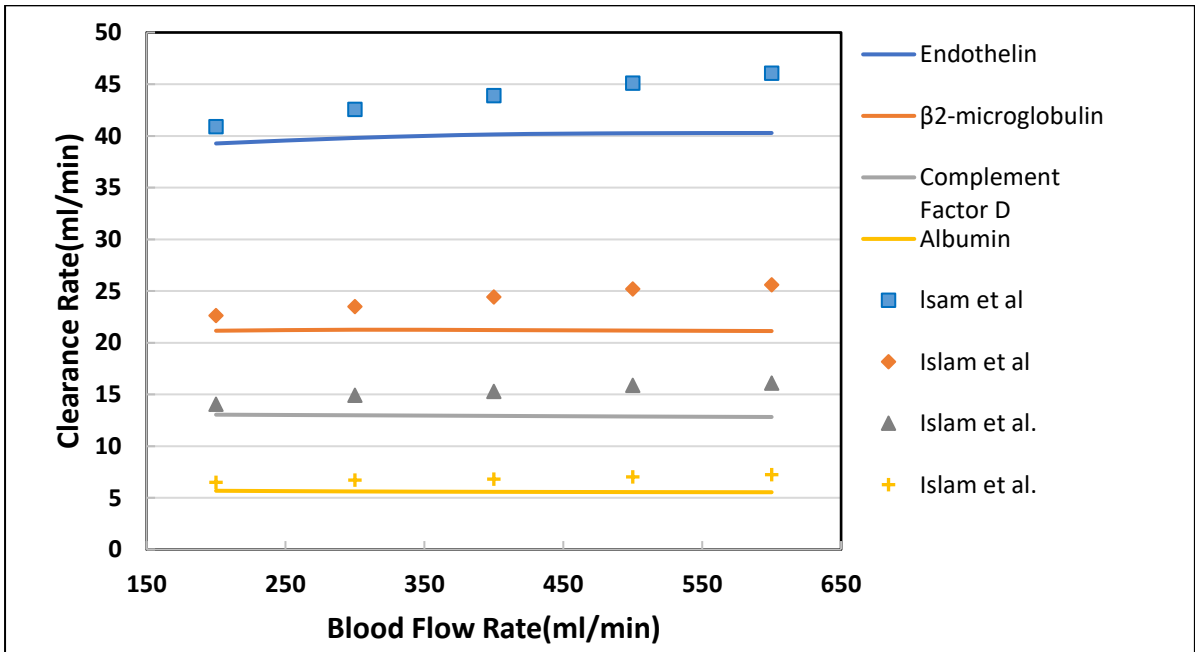


Figure 12. Model predicted (solid lines) vs in vivo and in silico (symbols) solute clearances plotted against varying blood flow rate at $Q_D=500\text{ml/min}$

Table 4. Maximum percentage difference of this model with literature data at varying blood flow rate [16]

Solutes	Blood flow rate(ml/min)	Model-predicted clearance(ml/min)	Islam et al. clearance(ml/min)	Percentage Difference
Urea	300	247.77	244.62	1.28
Glucose	200	152.50	147.68	3.26
Endothelin	600	40.28	46.08	12.52
β 2-Microglobulin	600	21.13	25.57	17.36
Complement	600	12.81	16.07	20.28
Factor D				
Albumin	600	5.54	7.22	23.33

Figure 13 and 14 show the variation in clearance rate with dialysate flow rate. A good agreement was found between the model-predicted and Islam et al. in-silico results [16]. The trend of increase in clearance with dialysate flow is also validated by comparing it with Revaclear Max dialyzer experimental (reported in Bhimani et al. [53]) and Donato et al. in-silico results [44]. The difference between Revaclear Max and model-predicted data is due lack of comprehensive dataset of module parameter values needed for model predictions. The concentration gradient also increases by increasing the dialysate flow rate Q_D that ultimately enhance the clearance rate of urea and glucose as observed in figure 13. The behavior of large size molecules in figure 14 is similar to their behavior in figure 12, and the reason of low diffusivity of large size molecules across the membrane despite of high concentration gradient lies in the high values of steric hinderance H and friction coefficient $F(p)$.

Effect of blood and dialysate flow rate on clearance show that clearance efficiency is nearly proportional to flow rates for low value of Q_B and Q_D but clearance increases more rapidly at high blood flow rate. For each solute, the clearance ultimately achieves a maximum, independent of the flow rate as C_S has approached C_g , gel concentration or solubility limit. This maximum clearance value is achieved faster for high molecular weight solutes.

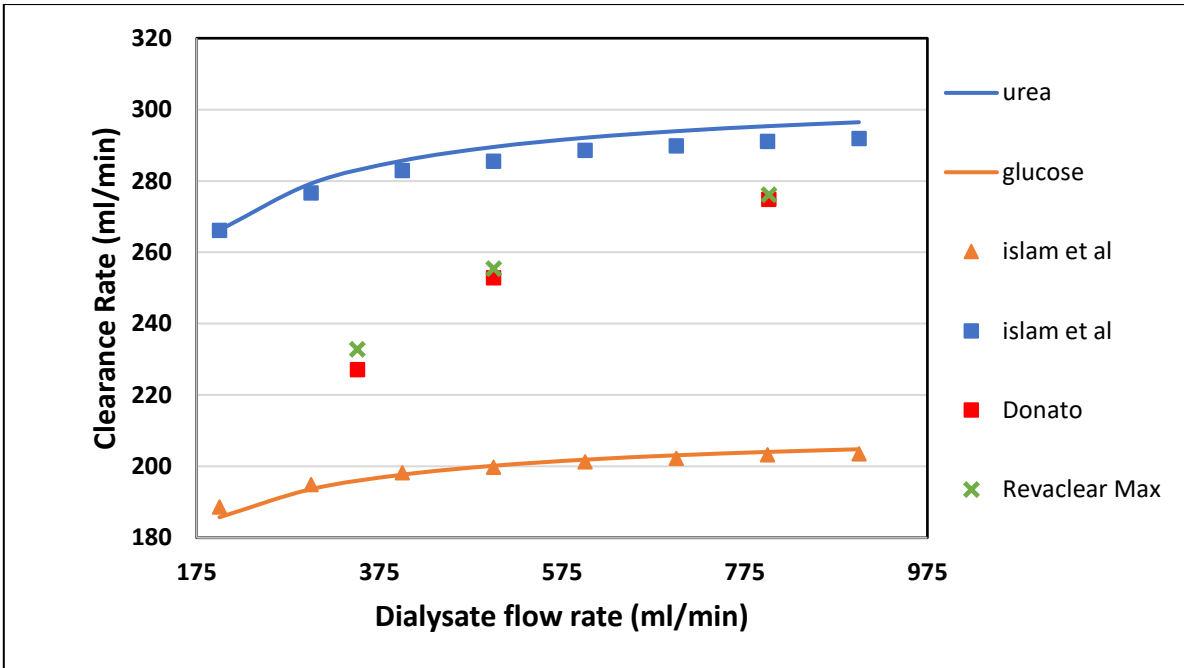


Figure 13. Model predicted (solid lines) vs in vivo and in silico (symbols) solute clearances plotted against varying dialysate flow rate at $Q_B=400\text{ml/min}$

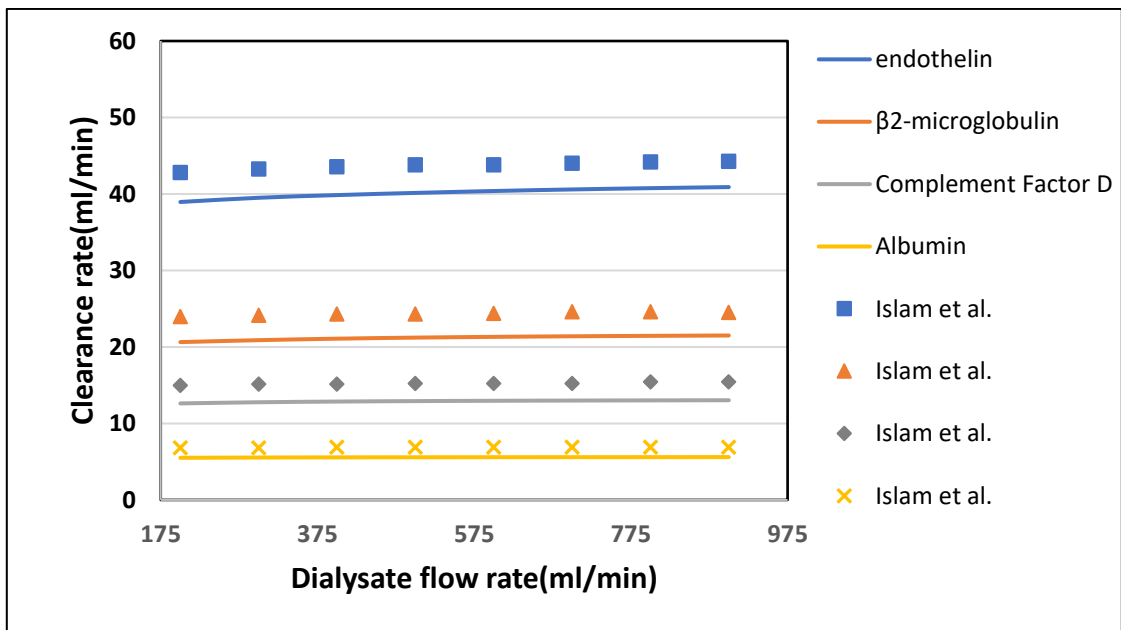


Figure 14. Model predicted (solid lines) vs in vivo and in silico (symbols) solute clearances plotted against varying Dialysate flow rate at $Q_B=400\text{ml/min}$

Table 5. Maximum percentage difference of this model with literature data at varying dialysate flow rate [16]

Solutes	Dialysate flow rate(ml/min)	Model-predicted clearance(ml/min)	Islam et al. clearance(ml/min)	Percentage Difference
Urea	900	296.45	291.84	+1.57
Glucose	200	185.75	188.60	+1.51
Endothelin	200	38.95	42.82	-9.03
β 2-Microglobulin	200	20.63	23.95	-13.86
Complement Factor D	300	12.77	15.15	-15.71
Albumin	400	5.56	6.89	-19.30

4.2 Effect of module geometry on solute clearances

Effect of different module dimensions on clearance rate of solute was investigated. It was observed that fiber length, radius and pore size have significant impact on the clearance rate. Therefore, these parameters are discussed in detail.

4.2.1 Effect of fiber length on clearance rate

The fiber length was varied from 270mm to 540mm while keeping blood flow rate $Q_B=300\text{ml/min}$ and dialysate flow rate $Q_D=540\text{ml/min}$. From figure 15, it is evident that the clearance rate of urea and glucose rises rapidly by increasing the length of the fiber. Similarly, in figure 16, the clearance rate of Endothelin and β 2-Microglobulin is doubled by varying the length from 270mm to 540mm. This increase has to be completely attributed to increase in total surface area of the hollow fibers. However, the albumin clearance is not affected much due to large size of its molecules.

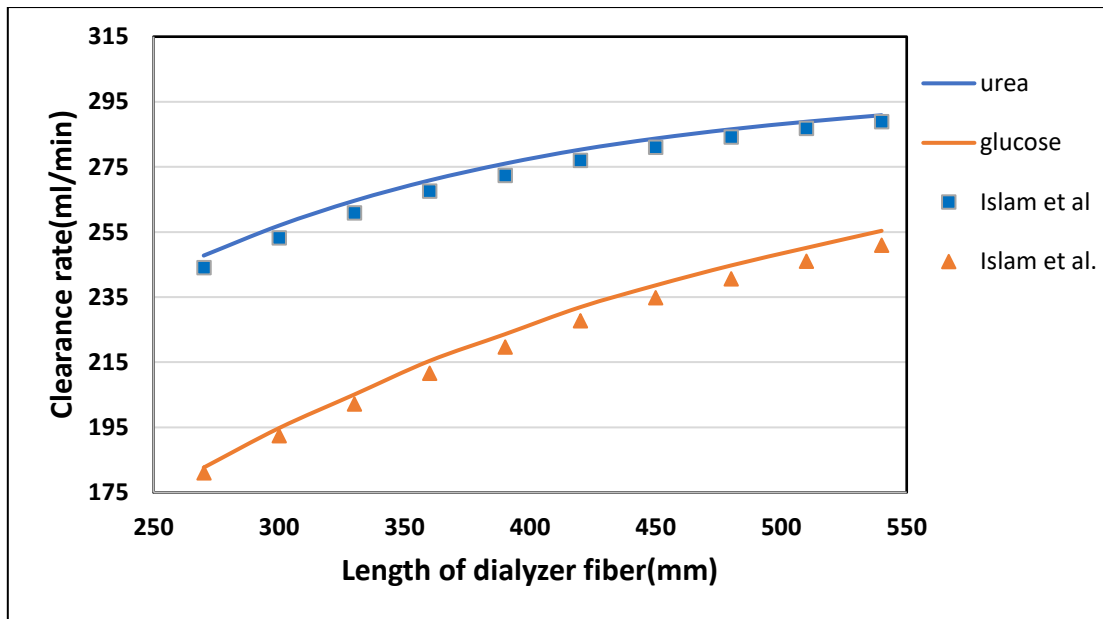


Figure 15. Clearance rate of low molecular weight solutes (urea, glucose) plotted against varying length of the dialyzer at $Q_B=300\text{ml/min}$ and $Q_D=500\text{ml/min}$

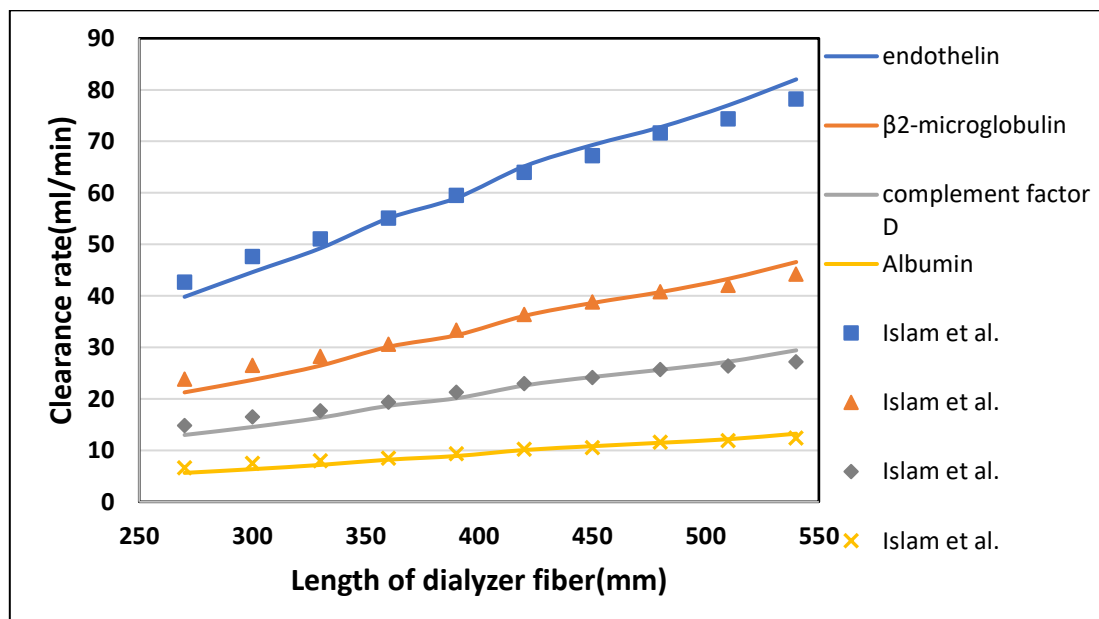


Figure 16. Clearance rate of high molecular weight solutes plotted against varying length of the dialyzer at $Q_B=300\text{ml/min}$ and $Q_D=500\text{ml/min}$

Table 6. Maximum percentage difference of this model with literature data at varying dialyzer fiber length [21]

Solutes	fiber length(mm)	Model-predicted clearance(ml/min)	Islam et al. clearance(ml/min)	Percentage Difference
Urea	270	247.77	244	+1.54
Glucose	420	231.93	227.68	+1.86
Endothelin	270	39.80	42.70	-6.79
β 2-Microglobulin	300	23.67	26.54	-10.81
Complement Factor	270	12.89	14.80	-12.90
D				
Albumin	270	5.61	6.63	-15.38

4.2.2 Effect of fiber radius on clearance rate

Radius determines the opening of fiber cavity throughout the fiber length in axial direction. It was varied from 0.1mm to 0.2mm while keeping the blood flow rate $Q_B=300\text{ml/min}$ and dialysate flow rate $Q_D=500\text{ml/min}$. From figure 17, it was observed that the clearance rate of solutes also increased by increasing the radius of fibers. This can also be attributed to overall increase in surface area of the membrane. Figure 18 shows that clearance of middle to large size molecules (from endothelin to albumin) also rises with increase in the radius of fiber but effect becomes negligible as the size of molecule increases.

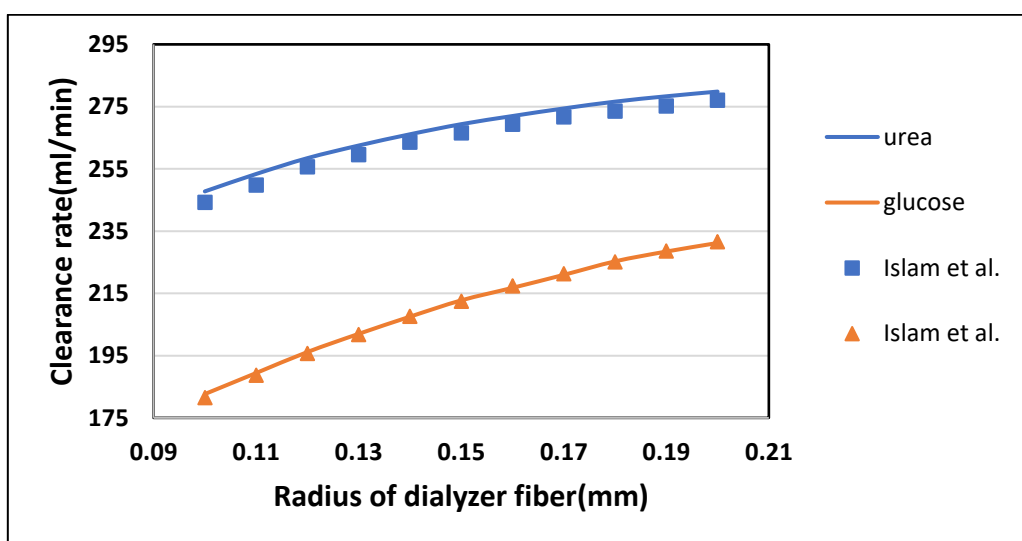


Figure 17. Clearance rate of low molecular weight solutes plotted against varying radius of the dialyzer at $Q_B=300\text{ml/min}$ and $Q_D=500\text{ml/min}$

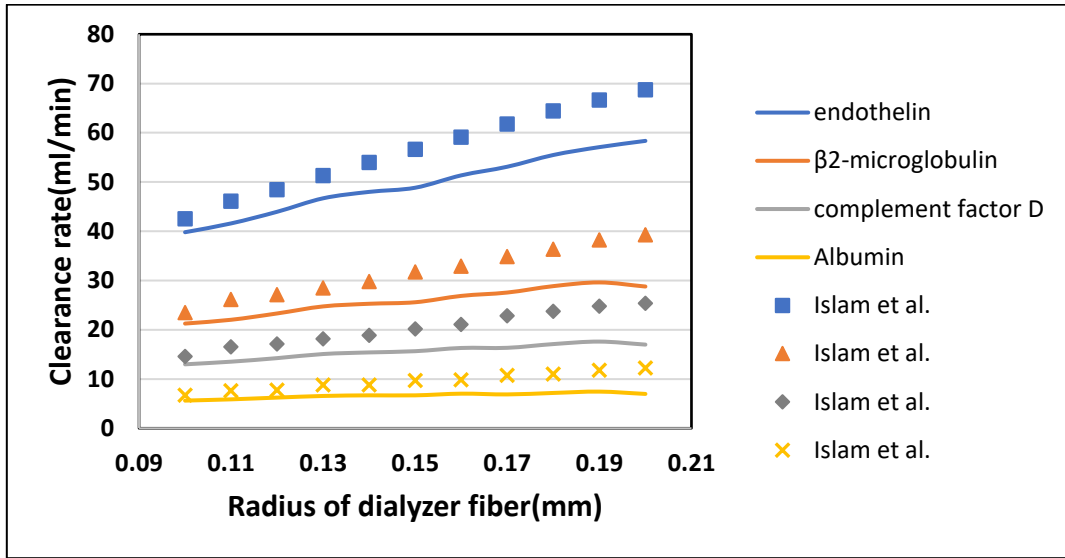


Figure 18. Clearance rate of high molecular weight solutes plotted against varying radius of the dialyzer at $Q_B=300\text{ml/min}$ and $Q_D=500\text{ml/min}$

Table 7. Maximum percentage difference of this model with literature data at a varying radius of dialyzer fiber [16]

Solutes	fiber radius(mm)	Model-predicted clearance(ml/min)	Islam et al. clearance(ml/min)	Percentage Difference
Urea	0.1	247.77	244.18	+1.47
Glucose	0.1	182.65	181.48	+0.64
Endothelin	0.2	58.34	68.75	-15.14
β 2-Microglobulin	0.2	28.77	39.302	-26.79
Complement Factor D	0.2	16.98	25.39	-33.11
Albumin	0.2	6.97	12.23	-42.95

4.2.3 Effect of fiber aspect ratio

The ratio between fiber length and diameter depict the interplay between fiber dimensions and clearance rate. This ratio is called fiber aspect ratio and it is an important parameter to determine the optimum length and radius of the fiber. Figure 19 shows that as the fiber aspect ratio increases, the clearance rate also increases. It confirms that if length of the fiber increases while keeping the radius constant the clearance rate will increase. The difference between the

model predicted and Donato et al. data is due to the fact that the impact of ultrafiltration enhances the clearance efficiency and ultrafiltration flow rate is not included in current model.

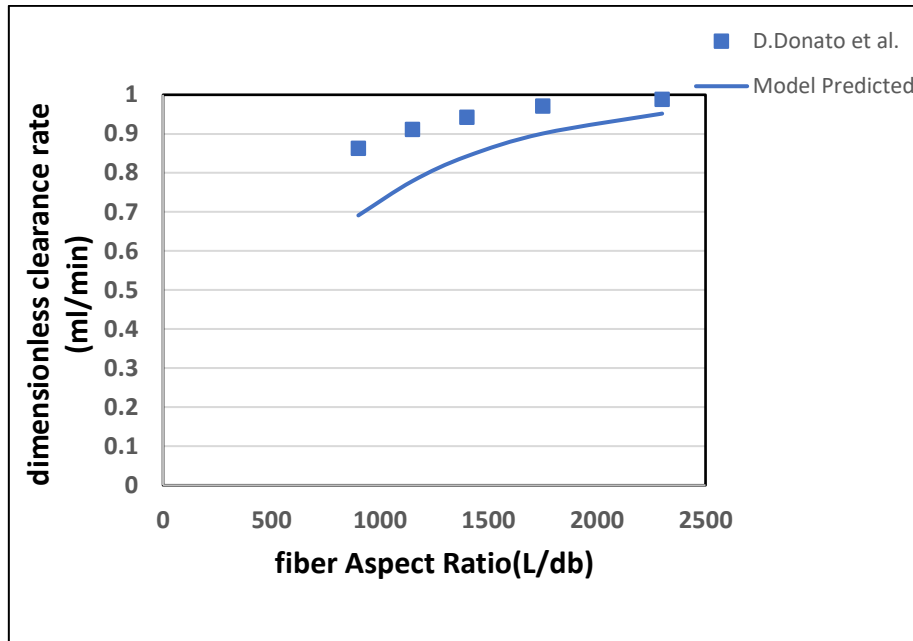


Figure 19. Dimensionless urea clearance rate plotted with varying fiber aspect ratio

Table 8. Maximum percentage difference of this model with literature data at varying aspect ratio of dialyzer fiber [16]

Solutes	fiber aspect ratio (--)	Model-predicted clearance(ml/min)	D.Donato et al. clearance(ml/min)	Percentage Difference
Urea	900	0.6911	0.8625	-15.52

4.2.4 Effect of skin layer pore size on clearance rate

In figure 20, it can be seen that the clearance rate increases more rapidly from 10nm to 20nm. After 20nm, as the pore size of the skin layer becomes equal to the middle layer, the clearance rate become independent of pore diameter. Since the pore size increases from inner (skin) layer to the outer (bulk) layer, therefore skin layer, that is directly in contact with blood, plays a vital role in improving the permeability of different solutes. Skin layer has the smallest average pore size among the three layers. A small change in the skin layer pore size produce a large impact on clearance of toxins. Although increasing the pore size of skin layer enhance the clearance of small size molecules (urea and glucose) but it also adds a huge increment to diffusion of

albumin. This happens due to decrease in steric hindrance S_D and friction coefficient $F(p)$ of the skin layer.

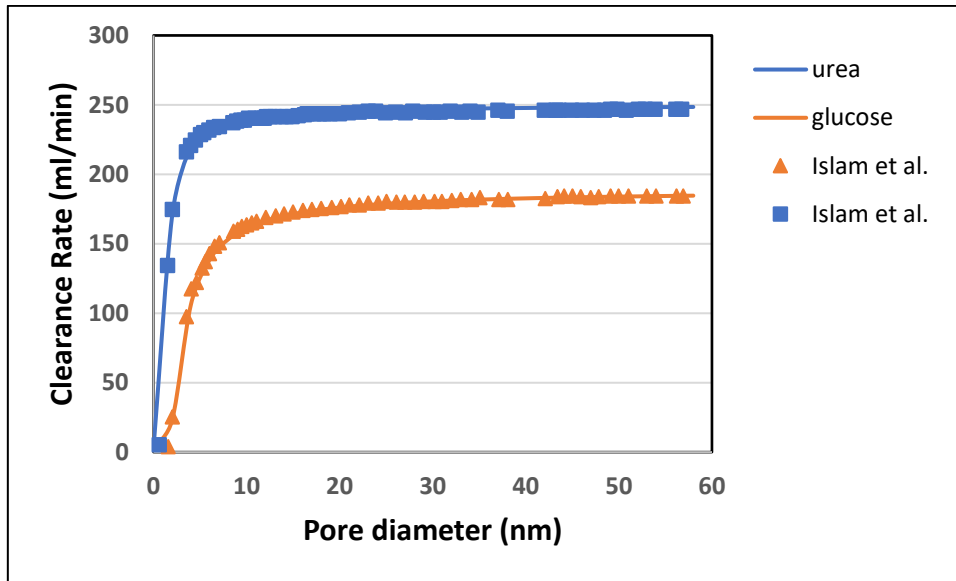


Figure 20. Effect of pore diameter on clearance rate of urea and glucose

Figure 21 shows that when pore diameter increased beyond 20nm the Albumin molecules escaped more rapidly. However, Albumin rejection is still very high in the limit of middle 1 to 20 nm with improved clearances of middle size molecules.

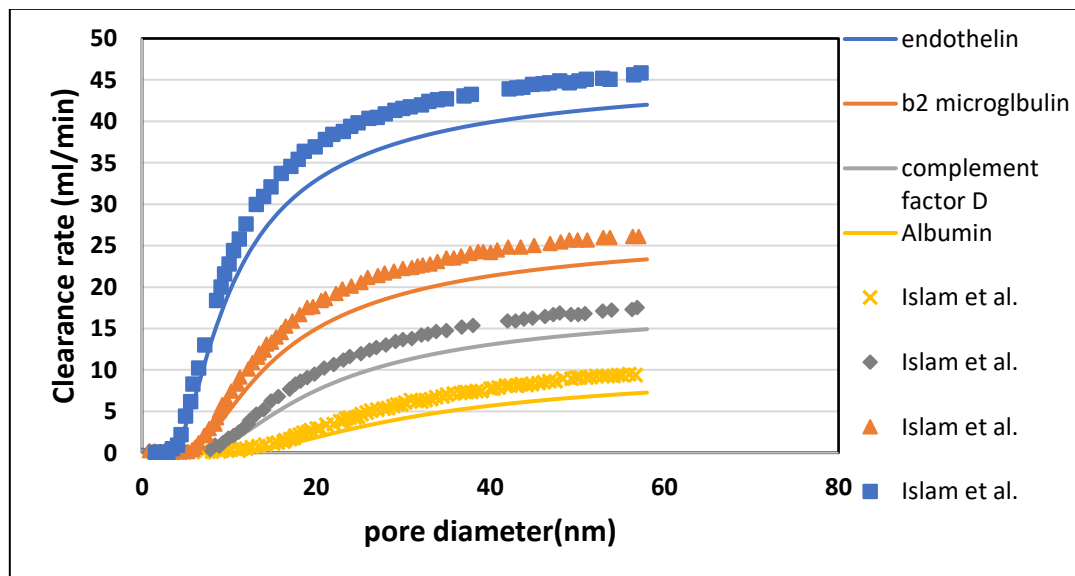


Figure 21. Effect of pore diameter on clearance rate of large molecular weight (LMW) molecules

This shows that increasing pore size up to 20nm (but not beyond that) provide better clearance of the toxins, with bearable loss of Albumin.

Table 9. Maximum percentage difference of this model with literature data at varying pore diameter of dialyzer fiber [16]

Solutes	pore dia (nm)	Model-predicted clearance(ml/min)	Islam et al. clearance(ml/min)	Percentage Difference
Urea	-	-	-	-
Glucose	-	-	-	-
Endothelin	58	42.00	45.81	8.32
β 2-Microglobulin	56	23.18	26.08	11.12
Complement	56	14.76	17.29	14.63
Factor D				
Albumin	56	7.13	9.35	23.74

CHAPTER 5

DEVELOPMENT OF A STAND-ALONE APPLICATION

5.1 Motivation for building a stand-alone application

Due to little communication between the in vitro and in silico research there is no efficient tool for the wet lab workers that enables them to rigorously determine the effect of membrane properties and other process parameters on clearance efficiency of dialyzer module. This void hinders to develop a membrane module that efficiently mimics the function of human kidney. To the best of authors' knowledge, COMSOL Inc. has developed an application that enable to study the effect of few membrane properties and design parameters on module clearance efficiency, but it does not mimic the transport phenomena associated with dialyzers merely because of the simplicity of the mathematical model [46]. Nevertheless, it inspires towards the development of a better application that could reduce the cost of R&D needed to optimize membrane properties and module design.

5.2 Introduction to Application Builder

Due to complexity of the simulation models, only researchers, having expertise in computational analysis, can use the COMSOL packages. To make this dialyzer model useful for research worker and medical doctors, COMSOL Application Builder provides a solution. Through COMSOL Application Builder, the modeling and simulation expert can develop a ready-to-use stand-alone application, that provides very precise user interphase.

5.3 Switching the COMSOL Environment

Switching from the Model Builder to Application Builder environment, introduce us with the user interphase of COMSOL Multiphysics Application Builder. The main entities of Application Builder interphase are shown in figure 23. Two major tools to build an application are:

- Form editor
- Method editor

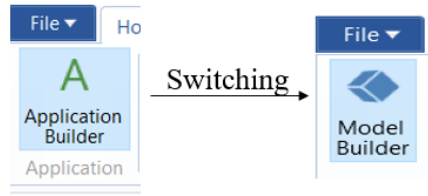


Figure 22. Switching from Model Builder to Application Builder

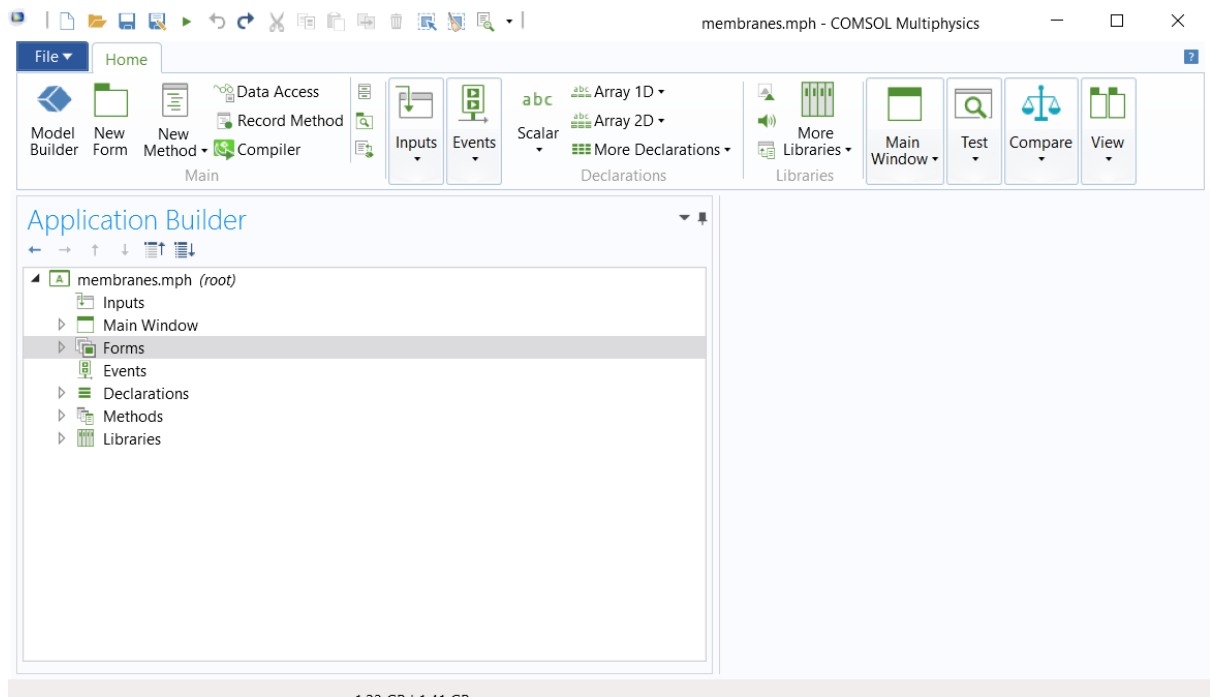


Figure 23. Application Builder environment of COMSOL Multiphysics

5.4 Development of Forms

Nine forms were created to build the user interphase of the application as shown in figure 24.

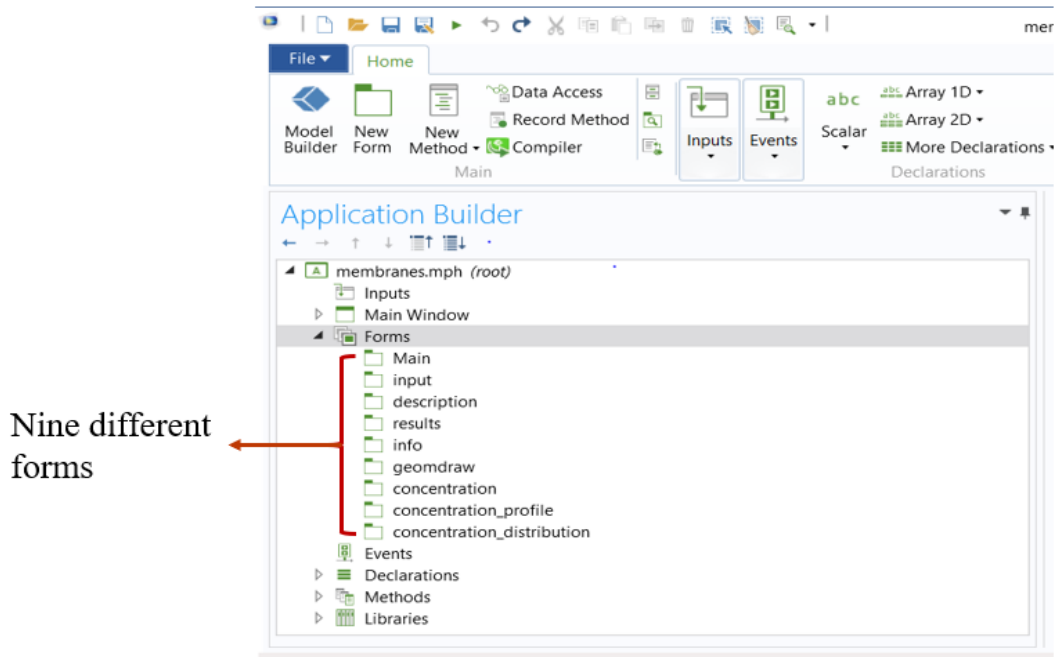
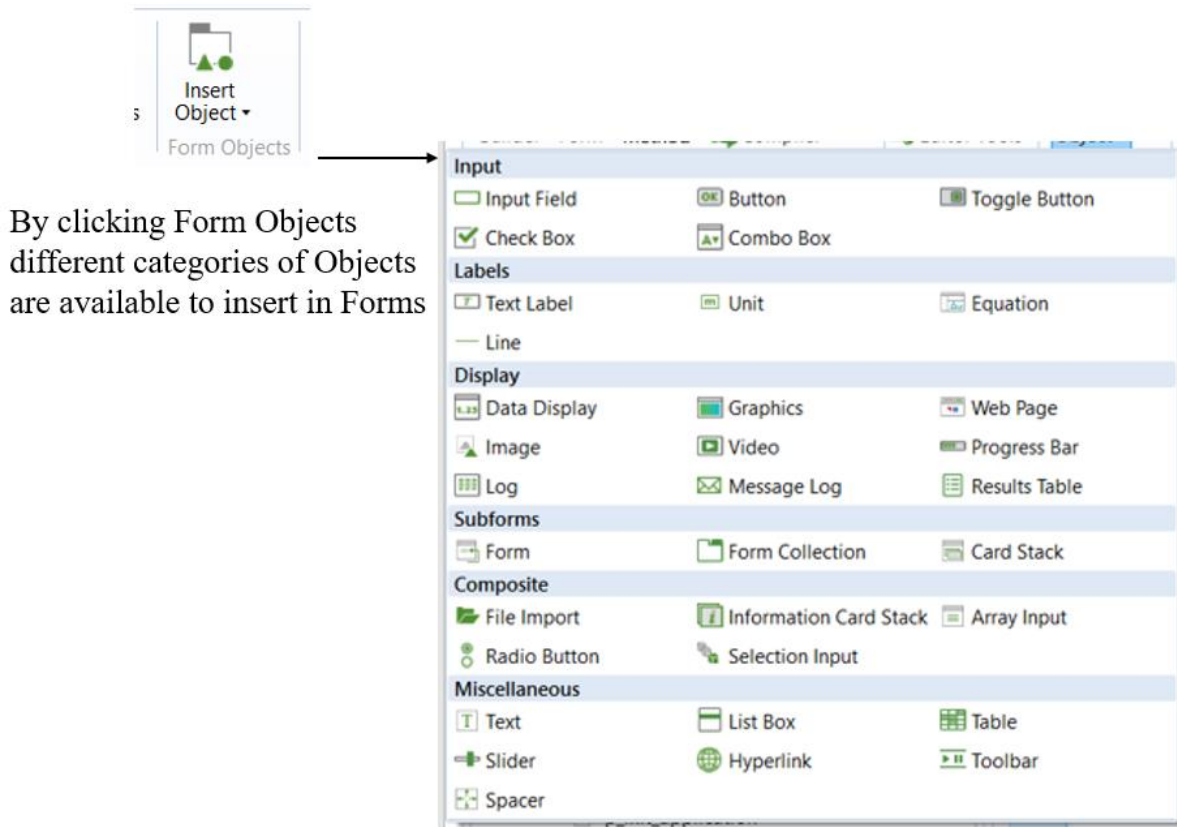


Figure 24. Forms created to build the application

For development of these forms the **Form Objects** available on ribbon are used. These **Form Objects** are shown in figure 25. Each **Form Object** has its own settings window, that opens when an object is included in the **Form**. The **Form** is always divided into desired number of rows and columns to create cells for **Form Objects**.



By clicking Form Objects different categories of Objects are available to insert in Forms

Figure 25. Form Objects available in COMSOL Application Builder to develop Forms

5.4.1 Main Form

Main form includes all the other forms created, to make a complete display of the user interphase. Following **Form Objects** were used to make eight different forms available on the user interphase.

- **Text Labels:** Four **Text Labels** were used to display different text as shown in figure 26 and 27. Text label 1 is used to display heading – Inputs & Results. Text Label 2 is used to display heading – Graphics & Results. Text Label 3 and 4 are used to put description and acknowledgements.
- **Form Collections:** Two **Form Collections** were used to make collection of certain forms in the same cell. From Figure 26 and 27, it can be seen that **Form Collection1** was used to display **input**, **description** and **results** form and **Form collection 2** was used to combine **geodraw**, **concentration**, **concentration profile** and **concentration distribution** forms.
- **Image:** It was used to display the logo of SCME NUST (figure 27).

Main

Input & Results

Text Label 1

Input Parameters

Membrane Parameters

inner radius of the fiber, R1 0.10 mm

Radius upto outer layer, R2 0.145 mm

Radius of concentric permeate channel, R3 0.210 mm

length of the fiber, H 270 mm

tortuosity 2.27

porosity of skin layer .1

average dia of skin layer pores 39.5 nm

number of fibers, n 12000

Process Parameters

Inlet concentration, c0 1 mol/liter

blood flow rate, Qb 300 ml/min

dialysate flow rate, Qd 500 ml/min

Description

Form Collection 1

Results

Urea clearance rate	0.001235	ml/min
Glucose Clearance rate	0.001235	ml/min
Endothelin Clearance rate	0.001235	ml/min
β 2-microglobulin clearance rate	0.001235	ml/min
Complement Factor D	0.001235	ml/min
Albumin	0.001235	ml/min
Packing Density	0.001235	

Figure 26. Form Objects used in Left-half of the Main form

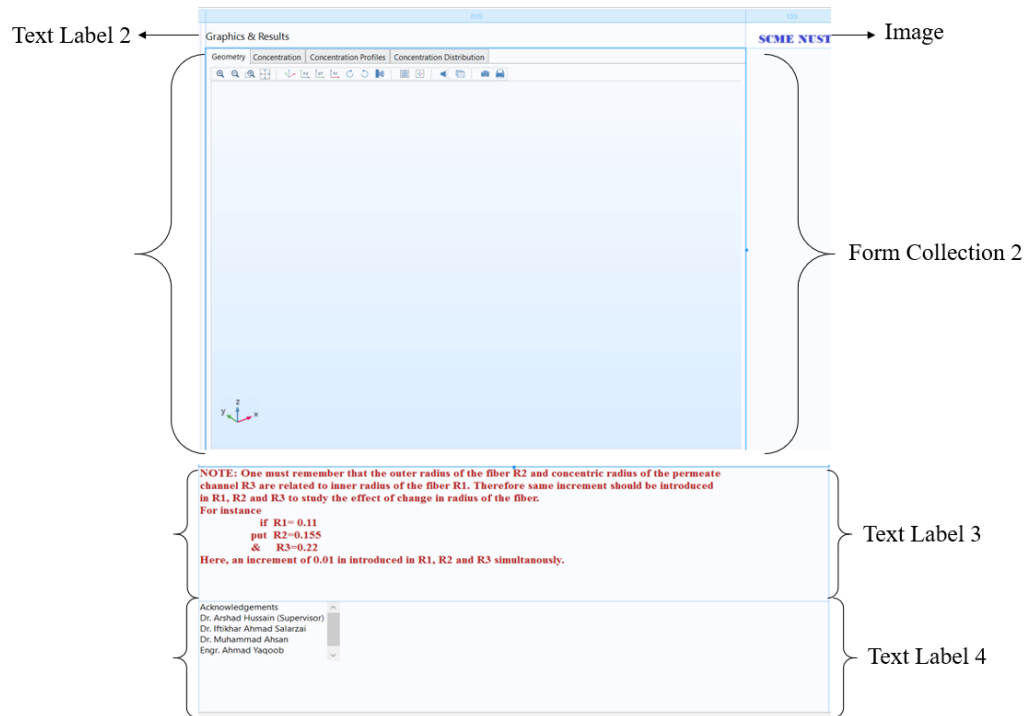


Figure 27. Form Objects used in Right-half of the Main form

5.4.2 Input Form

It was created to display all the input parameters to the user. This form was developed with four different **Form Objects**:

- **Line:** Used to put headings of process parameters and membrane parameters (Figure 28).
- **Text Label:** Used to put names of parameters (Figure 28).
- **Input Field:** Used to provide a numeric text box to user for putting value of parameter (Figure 28).
- **Unit:** Used to display units of parameters (Figure 28).

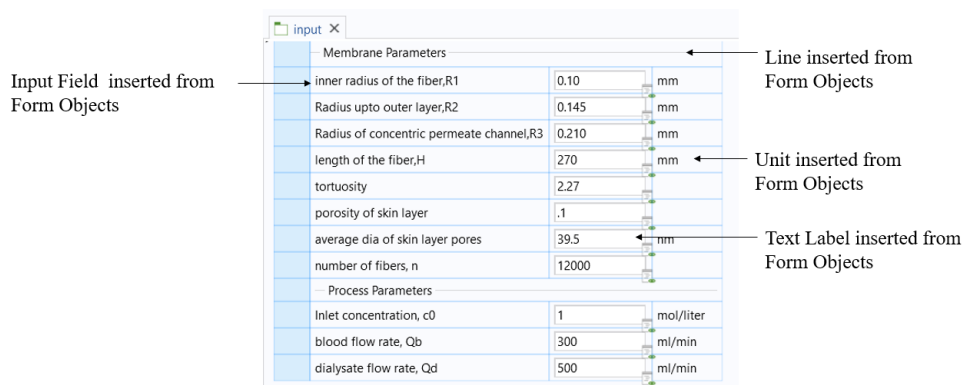


Figure 28. The Input Form developed with **Form Objects**

5.4.3 Description form

To display the 2-D axisymmetric model of membrane a **description form** was created, and **Image** was inserted in this form through **Form Objects** (Figure 29).

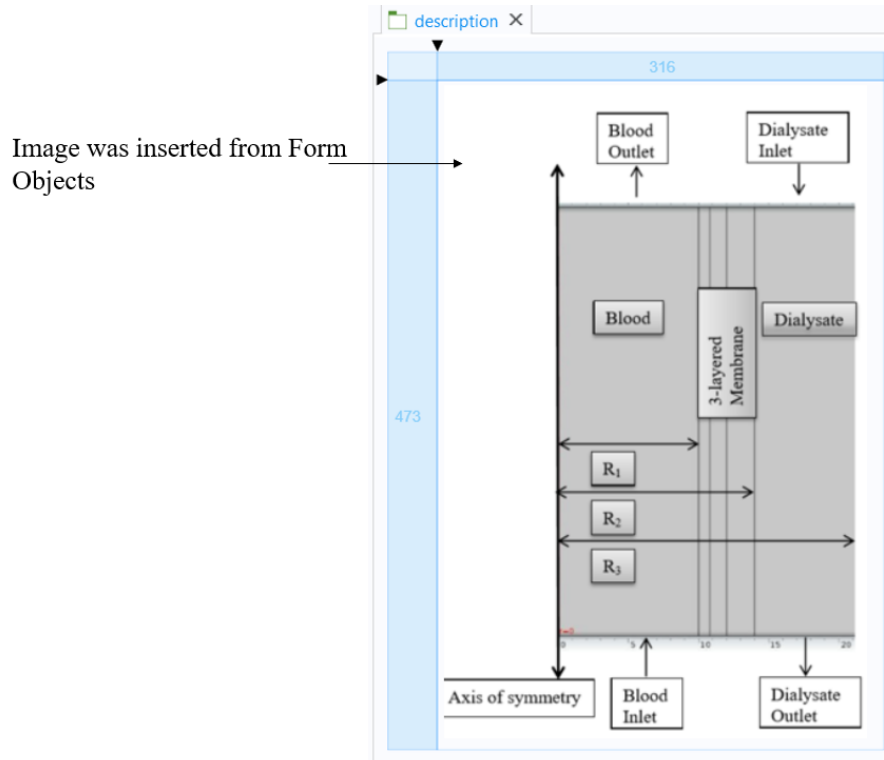


Figure 29. Description form developed with **Form Object**

5.4.4 Results form

It was created to display the clearance rates of all the toxins. This form was developed with three type of **Form Objects**.

- **Text Label:** It was used to insert the names of all the output parameters as shown in Figure 30.
- **Data Display:** It was used to provide a place holder to the numeric value of output (Figure 30).
- **Unit:** It was used to display units of output parameters (Figure 30).

	199	181	51
Urea clearance rate	0.001235		ml/min
24 Glucose Clearance rate	0.001235		ml/min
Endothelin Clearance rate	0.001235		ml/min
β2-microglobulin clearance rate	0.001235		ml/min
Complement Factor D	0.001235		ml/min
Albumin	0.001235		ml/min
Packing Density	0.001235		

Text Labels inserted from Form Objects Data Display inserted from Form Objects Units inserted from Form Objects

Figure 30. The **Result Form** developed with **Form Objects**

5.4.5 Info form

It was created to show the expected computation time. Four **Form Objects** were included here as shown in figure 31.

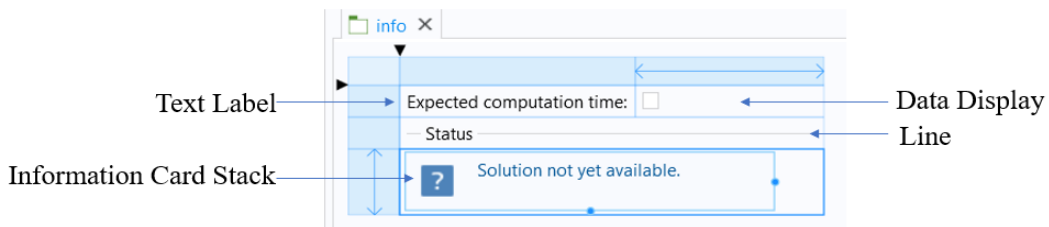


Figure 31. Info form developed with **Form Objects**

5.4.6 Geodraw form

It was created to provide a place holder to concentration, concentration profile and concentration distribution. The **Graphics** was added from **Form Objects** to set the background and tool bar of graphics window. It can be seen in figure 32 that the geodraw, concentration, concentration profile and concentration distribution form were created in the same cell to keep the graphical results in the graphics window.

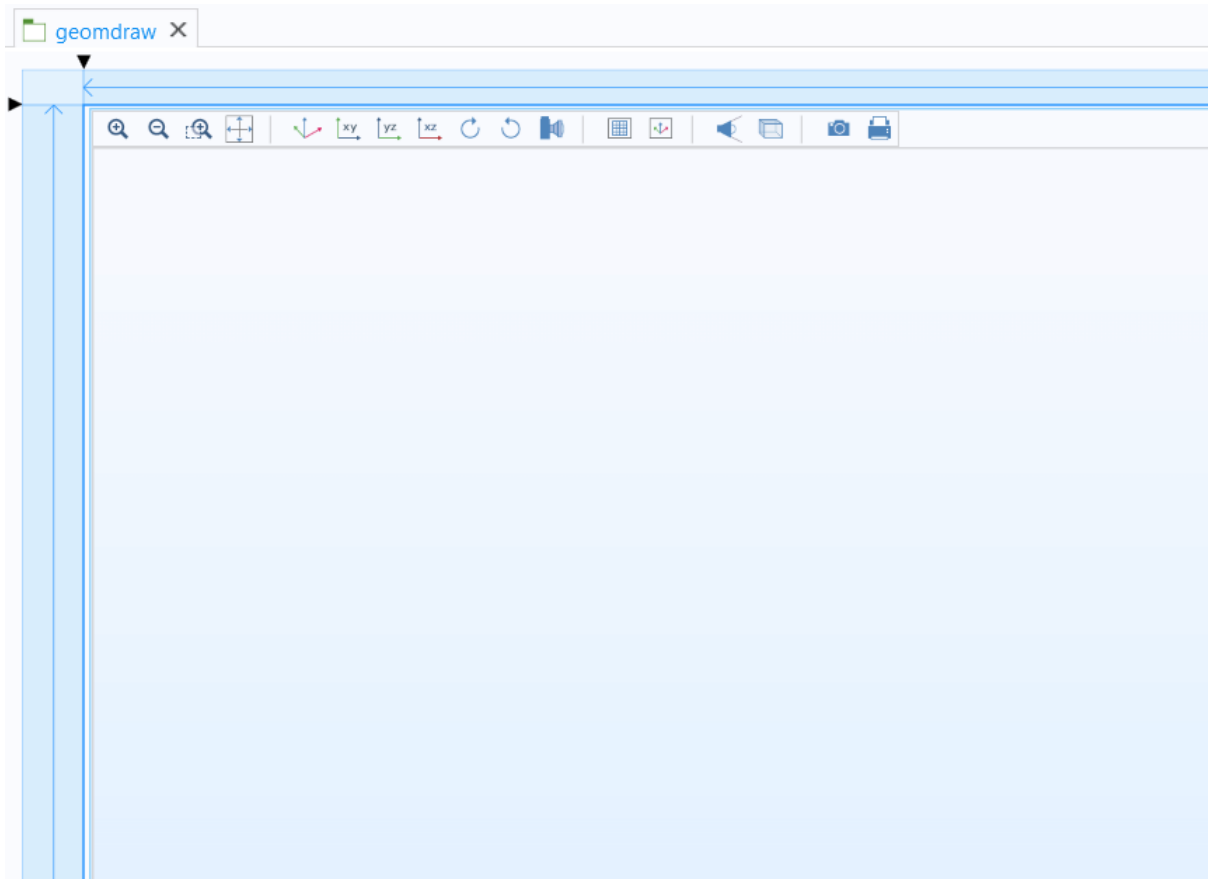


Figure 32. Geodraw developed with **Form Object**

5.5 Development of Methods

Methods is an important node available under the **Application Builder** window, as it can be used to execute loops and run actions that are not part of typical run commands of model tree nodes. **Methods** node consists of sub nodes called **New Method**. It can be seen in figure 33, five **New Method** nodes were created to build a path of various actions for this application.

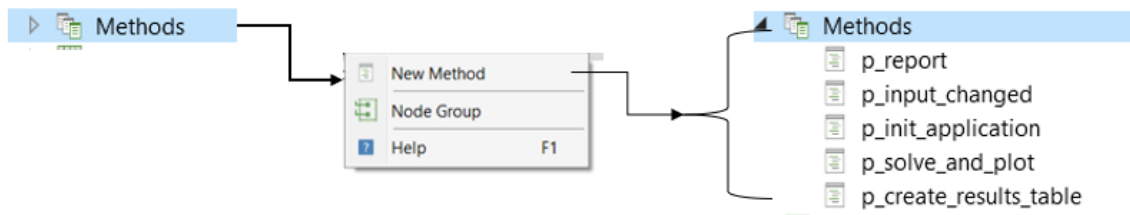


Figure 33. **New Method** nodes created to build a series of actions during application run.

5.5.1 p_report Method

This method node was created for automatic generation of a report, based on recently executed model results. To create such a report the basic commands were given in the **Report** node of the model building environment, available under the **Model Builder** window, as shown in figure 34. The commands written in **New Method** node, named **p_report**, to make this report available for the user, are shown in figure 35.

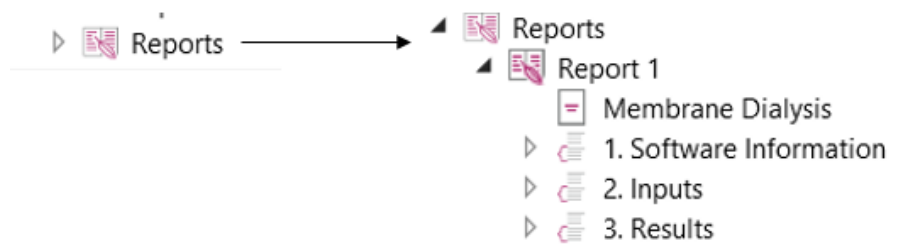


Figure 34. Report nodes created in model building environment to set the format and features of report

```
p_report X
1 if (!solution_state.equals("solutionexists")) {
2   alert("New input data. Compute to update results first.");
3 }
4 else {
5   model.result().report("rpt1").run();
6 }
```

Figure 35. if-else loop used to generate the report of results in application

5.5.2 p_input_changed Method

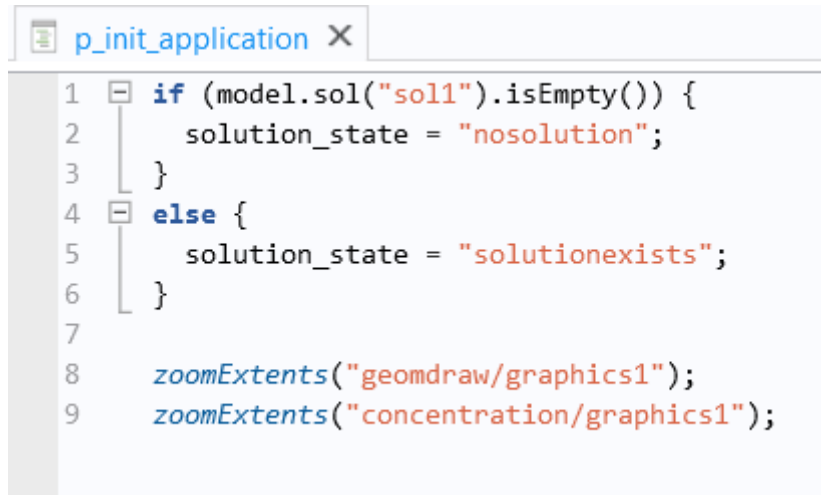
This method was created to ensure that the input will change only if the solution exist on the given input values. The code of this node is shown in figure 36.

```
p_input_changed X
1 if (solution_state.equals("solutionexists")) {
2   solution_state = "inputchanged";
3 }
```

Figure 36. Code written in the **p_input_changed** node

5.5.3 p_init_application Method

This method node was created to give sequence to the result plots in the graphics window. The code written for this purpose is shown in figure 37.



```
1  if (model.sol("sol1").isEmpty()) {  
2      solution_state = "nosolution";  
3  }  
4  else {  
5      solution_state = "solutionexists";  
6  }  
7  
8  zoomExtents("geomdraw/graphics1");  
9  zoomExtents("concentration/graphics1");
```

Figure 37. Code written in the **p_init_application** node

5.5.4 p_solve_and_plot Method

This method include code to solve and plot the exclusive results, needed in the graphics window, on changing the input. This will reduce the run time of the application as it will only work on the execution of specific plots. The code written in this regard is shown in figure 38.

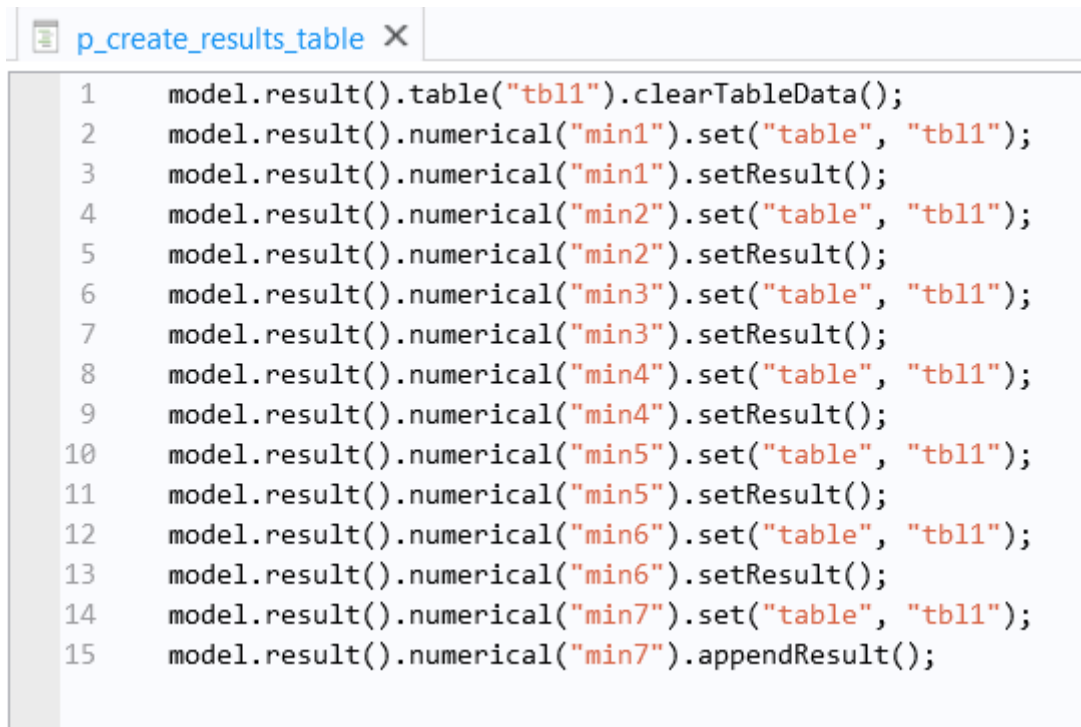


```
1  model.study("std1").run();  
2  solution_state = "solutionexists";  
3  
4  useGraphics(model.result("pg116"), "concentration/graphics1");  
5  useGraphics(model.result("pg122"), "concentration_profile/graphics1");  
6  useGraphics(model.result("pg11"), "concentration_distribution/graphics1");  
7
```

Figure 38. Code written in the **p_solve_and_plot** node

5.5.5 p_create_result_table Method

This code was written to include tabular form of results in the report, generated when the application is executed.



```
1 model.result().table("tbl1").clearTableData();
2 model.result().numerical("min1").set("table", "tbl1");
3 model.result().numerical("min1").setResult();
4 model.result().numerical("min2").set("table", "tbl1");
5 model.result().numerical("min2").setResult();
6 model.result().numerical("min3").set("table", "tbl1");
7 model.result().numerical("min3").setResult();
8 model.result().numerical("min4").set("table", "tbl1");
9 model.result().numerical("min4").setResult();
10 model.result().numerical("min5").set("table", "tbl1");
11 model.result().numerical("min5").setResult();
12 model.result().numerical("min6").set("table", "tbl1");
13 model.result().numerical("min6").setResult();
14 model.result().numerical("min7").set("table", "tbl1");
15 model.result().numerical("min7").appendResult();
```

Figure 39. Code written in the `p_create_result_table` node

5.6 Development of the File Menu and Ribbon tab

The **Application Builder** window contains a node called **Main Window** that is used to develop **File Menu** and **Ribbon** tab for the application. The **File Menu** and **Ribbon** tab of the application was created by using sub-nodes of the **Main Window**. The procedure of this development process is shown in figure 40.

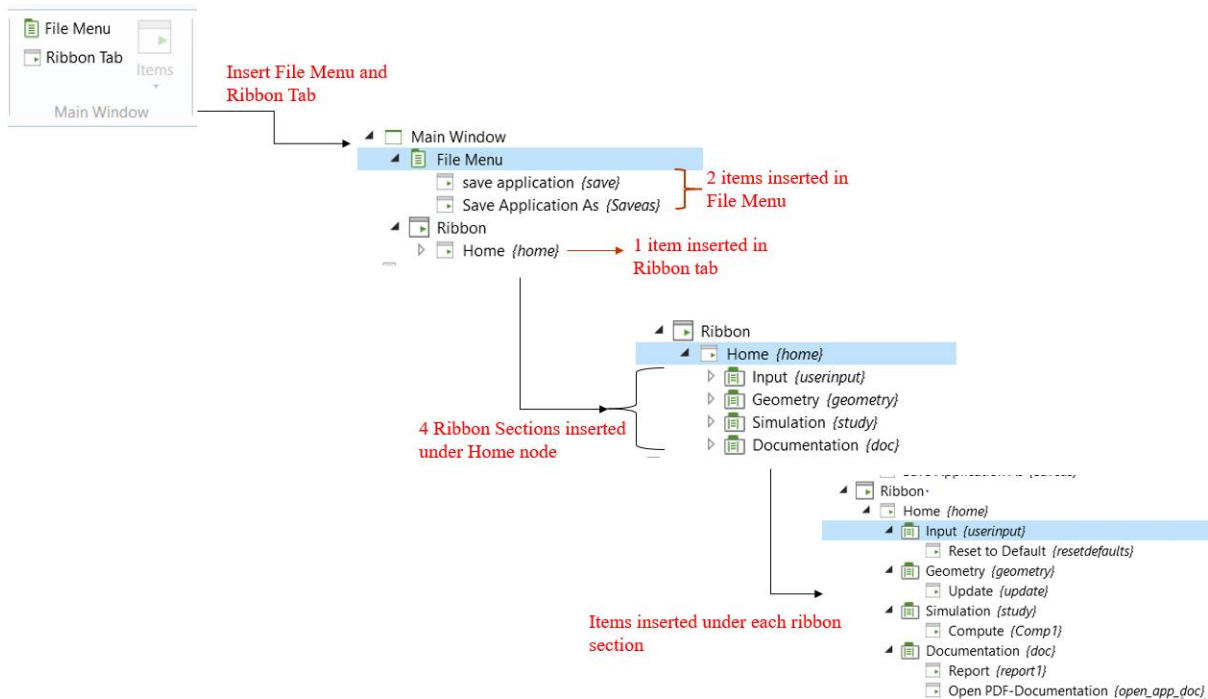


Figure 40. Step wise development of sections and sub-sections of **File Menu** and **Ribbon Tab**

5.6.1 Reset to Default item

This item, created under **Ribbon Section** named **Input**, was used to reset the values of all the input parameters to their default values. Following sequence of commands was given in the setting window of this **item**.

Command	Icon	Arguments
Set R1 of Parameters 1		0.1[mm]
Set R2 of Parameters 1		0.145[mm]
Set R3 of Parameters 1		.210[mm]
Set H of Parameters 1		270[mm]
Set tau of Parameters 1		2.27
Set ei of Parameters 1		0.1
Set dpin of Parameters 1		39.5[nm]
Set n of Parameters 1		12000
Set c0 of Parameters 1		1[mol/liter]
Set Q_b of Parameters 1		300[ml/min]
Set Q_d of Parameters 1		500[ml/min]
Build Geometry display		
Zoom extents		main/collection2/graphics1
p_input_changed		

Figure 41. Command sequence included in **Reset to Default Item**

5.6.2 Update item

This item, created under **Ribbon Section** named **Geometry**, was used to update the geometry in the graphics window. Following sequence of commands was given in the setting window of this **item**.

Command	Icon	Arguments
Build Geometry display		
Plot Geometry display		
Zoom extents		geomdraw/graphics1

Figure 42. Command sequence included in **Update item**

5.6.3 Compute item

Compute is an **Item** created under the **Ribbon Section**, named **Simulation**, to execute the computational analysis output in a given sequence. The sequence of commands is shown in figure 43.











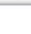
Command	Icon	Arguments
Build Geometry 1		
Build Mesh 1		
Plot Geometry display		geomdraw/graphics1
Zoom extents		geomdraw/graphics1
p_solve_and_plot		
Zoom extents		concentration/graphics1
Zoom extents		concentration_profile/graphics1
Zoom extents		concentration_distribution/graphics1
Reset current view		concentration_distribution/graphics1
p_create_results_table		
Set active_plot of String		concentration

Figure 43. Command sequence included in **Compute item**

5.6.4 Report item

Report is an **Item** created under the **Ribbon Section**, named **Documentation**, to generate the report based on output of computational analysis. The command for this is shown in figure 44.

Command	Icon	Arguments
p_report		

Figure 44. Command for report generation

5.6.5 Open PDF Documentation item

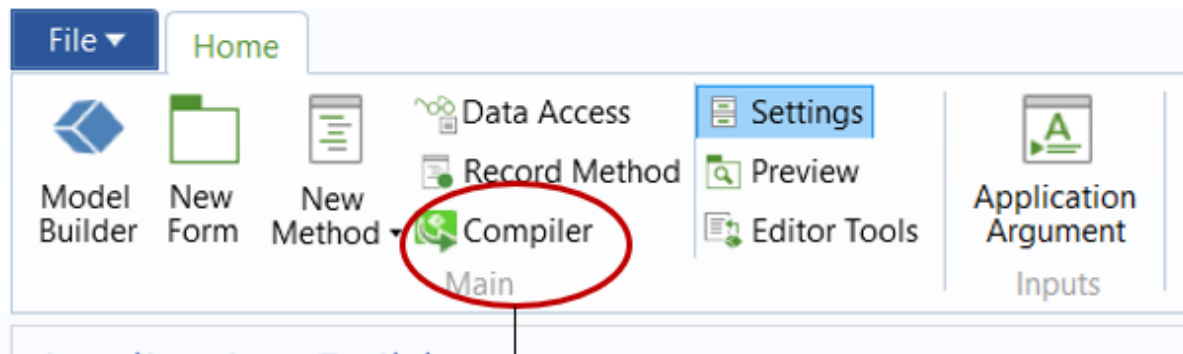
This item was created under the **Ribbon Section**, named **Documentation**, to see pdf document related to COMSOL Multiphysics Model. The command given in this section is shown in figure 45.

Command	Icon	Arguments
Open file		embedded:///comsol-models.chem....

Figure 45. Command to see associated PDF file

5.7 Compiler

COMSOL Compiler was used to convert the application into a stand-alone app that could be used independently without licensed software. The compiler is available on the ribbon of Application building window as shown in figure 46.



Compiler available on ribbon tab

Figure 46. Compiler to create a stand-alone application.

5.8 Comparison of Stand-alone Application with COMSOL Application

Figure 47. is showing the input and results window of the COMSOL and stand-alone application. It can be seen from the figure that stand-alone application determines the clearance rate of six different solutes ranging from smaller to large size molecules as well as packing density of the module fibers. However, the COMSOL application just determines the concentration of dialyzed blood. In the COMSOL application model, the liquid is not defined on blood and dialysate side. The membrane modeling is not considered in COMSOL application whereas the stand-alone version is based on a multi-layered membrane modeled with TPDM. The factors of tortuosity and porosity are not included in the COMSOL application whereas user can put these factors in stand-alone application. Table 10. is showing the values of parameters used to build the mathematical model of COMSOL application versus the values or model equation used for building stand-alone application. Its is evident from the Table 10. that stand-alone application is based on a detailed model of multi-layered membrane whereas the COMSOL application has no model to determine the effective diffusivity of membrane.

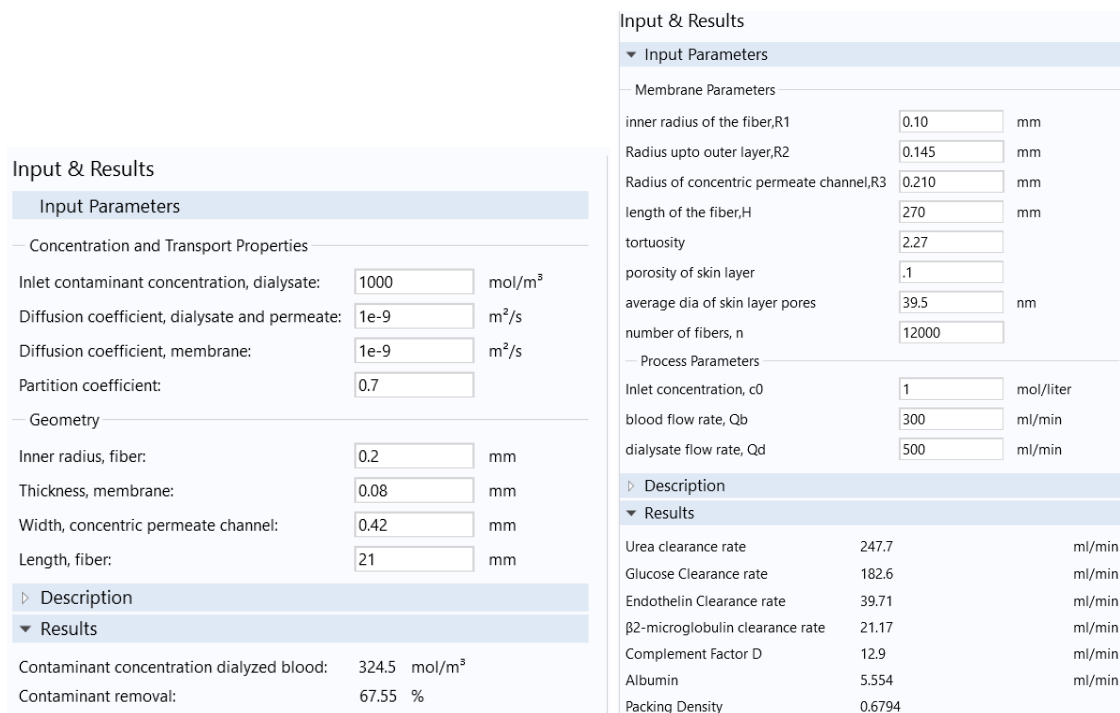


Figure 47. Comsol application window (Left side) vs Stand alone application window (Right side)

Table 10. Property Data set for COMSOL application vs Stand-alone Application

Property	COMSOL app. value	Stand-alone App value
Diffusion Coefficient of liquids, D	$10^{-9}\text{m}^2/\text{s}$	$D = 1.62 \times 10^{-12}(\text{MW}^{-0.552})$
Membrane Diffusion Coefficient, Dm	$10^{-9}\text{m}^2/\text{s}$	$D_{es,j} = \left(\frac{D_{s,i}\epsilon_{mj}}{\tau}\right)F(p)H_D$
Inner Radius of the hollow fiber, Rhf	0.2mm	0.10mm
Membrane Thickness, Lm	0.28mm	0.145mm
Width of the concentric permeate channel, Lpc	0.7mm	0.210mm
Length of the fiber, H	21mm	270mm
Average velocity of dialysate, Uav_dia	0.5mm/s	Determine by Continuity and Navier Stokes equation
Average velocity of permeate, Uav_per	0.8mm/s	Determine by Continuity and Navier Stokes equation

CONCLUSION AND FUTURE RECOMMENDATIONS

- Tortuous Pore Diffusion Model (TPDM) was used to describe mass transport through the dialyzer membrane. Porosity and tortuosity were incorporated in this model to achieve a better estimation of solute clearance across the membrane.
- The numerical results obtained from this model were found in good agreement with the experimental results. This observation suggest that this model can be used to optimize the design and process parameters of the dialyzer module.
- The proposed model gave insight of the effect of porous medium tortuosity on diffusion of different solutes.
- By increasing the blood flow, the model predicted value of urea and glucose clearance were found 1.28% and 3.26% more than the Islam et al. predicted values. Similarly, the percentage increase found in urea and glucose clearance rate by increasing the dialysate flow, fiber length and fiber radius was 1.55% and 0.4%; 1.54 and 1.86%; 1.47 and 0.6%, respectively.
- The clearance rate of urea was increased 37.71% of its initial value by increasing the fiber aspect ratio. Due to the high steric hinderance H and friction coefficient $F(p)$ the diffusion of large size molecules (i.e. endothelin, β 2-microglobulin, complement factor D and albumin) do not increase much.
- When the pore diameter increases from 10 to 20 nm the clearance rate of urea and glucose rise by 2.09% and 7.93% of their initial values. The results suggest that the pore diameter can not be increased beyond 20nm as it leads to loss of albumin molecules which cannot be tolerated.
- Since, the developed application is stand-alone, user doesn't need COMSOL software to run the application as it was required in previous application.
- The liquids on both blood and dialysate side were not defined in the COMSOL application whereas this application determine the clearance rate of six different solutes.

- Application is simulating a multilayered membrane modeled with TPDM, but membrane modeling was not considered in COMSOL application.

In current study we investigated the transfer of six different toxins ranging from low to high molecular weight by using equation of diffusion.

If we incorporate radial convection of solute by applying trans-membrane pressure difference it would enhance the clearance and remove the excess water during hemodialysis. This process is called hemodiafiltration.

References

- [1]. Lysaght, J.P., Boggs, D.R., and Taimisto, M.H. (1986) *Membranes in artificial organs, in Synthetic Membranes* (ed. M.B. Chenoweth), Hardwood Academic Publishers, Chur, Switzerland, pp. 100–117.
- [2]. Daugirdas, J. T., and P. G. Blake. "Ing. TS Handbook of dialysis." *Vascular access for Hemodialysis. Boston: Little, Brown and Company* (1994).
- [3]. Li, Norman N., Anthony G. Fane, WS Winston Ho, and Takeshi Matsuura, eds. *Advanced membrane technology and applications*. John Wiley & Sons, 2011.
- [4]. Hall, John E. *Guyton and Hall textbook of medical physiology e-Book*. Elsevier Health Sciences, 2010.
- [5]. Olson, Jeffrey Carter. "Design and modeling of a portable hemodialysis system." PhD diss., Georgia Institute of Technology, 2009.
- [6]. Bethesda, M. D. "National kidney and urologic diseases information clearing house." *NIH Publication* 8 (2005): 3925.
- [7]. Hedayat, A., J. Szpunar, N. A. P. Kumar, R. Peace, H. Elmoselhi, and A. Shoker. "Morphological characterization of the Polyflux 210H hemodialysis filter pores." *International journal of nephrology* 2012 (2012).
- [8]. Meyer, Timothy W., and Thomas H. Hostetter. "Uremia." *New England Journal of Medicine* 357, no. 13 (2007): 1316-1325.
- [9]. Triplitt, Curtis L. "Understanding the kidneys' role in blood glucose regulation." *The American journal of managed care* 18, no. 1 Suppl (2012): S11-6.
- [10]. Miyata, T., Oda, O., Inagi, R., "Beta 2-Microglobulin modified with advanced glycation end products is a major component of hemodialysis-associated amyloidosis", *J. Clin. Invest.* Volume 92, Issue 3, Pages 1243-52, 1993.
- [11]. Volanakis, J. E. & Narayana S. V., "Complement Factor D, a novel serine protease", *Protein Sci.*, Volume 5, Issue 4, Pages 553-564, 1996.
- [12]. Krieter, Detlef H., and Bernard Canaud. "High permeability of dialysis membranes: what is the limit of albumin loss?." *Nephrology Dialysis Transplantation* 18, no. 4 (2003): 651-654.
- [13]. Ikizler, T. Alp, Paul J. Flakoll, Robert A. Parker, and Raymond M. Hakim. "Amino acid and albumin losses during hemodialysis." *Kidney international* 46, no. 3 (1994): 830-837.
- [14]. Baker, Richard W. *Membrane technology and applications*. John Wiley & Sons, 2012.
- [15]. Islam, Md Shihamul, and Jerzy Szpunar. "Study of dialyzer membrane (Polyflux 210H) and effects of different parameters on dialysis performance." *Open J. Nephrol* 3 (2013): 161-167.
- [16]. Fresenius Medical Care FX100 [Online]. Available at: <https://www.freseniusmedicalcare.asia/en/healthcare-professionals/hemodialysis/dialyzers/fx-high-and-low-flux-dialyzers/>

- [17]. Ullah, Kifayat, Ghias Butt, Imtiaz Masroor, Kinza Kanwal, and Farina Kifayat. "Epidemiology of chronic kidney disease in a Pakistani population." *Saudi Journal of Kidney Diseases and Transplantation* 26, no. 6 (2015): 1307.
- [18]. Conrad, Steven A. "Hemodialysis and hemofiltration." *Wiley Encyclopedia of Biomedical Engineering* (2006).
- [19]. Merrill, J.P. (1961) *The artificial kidney*. Sci. Am., 205, 56
- [20]. Quinton, Wayne, David Dillard, and Belding H. Scribner. "Cannulation of blood vessels for prolonged hemodialysis." *ASAIO Journal* 6, no. 1 (1960): 104-113.
- [21]. Zydney, Andrew L. "Bulk mass transport limitations during high-flux hemodialysis." *Artificial organs* 17, no. 11 (1993): 919-924.
- [22]. Jaffrin, Michel Y. "Convective mass transfer in hemodialysis." *Artificial organs* 19, no. 11 (1995): 1162-1171.
- [23]. Akcahuseyin, Emin, W. A. Van Duyl, M. C. Vos, and H. H. Vincent. "An analytical solution to solute transport in continuous arterio-venous hemodiafiltration (CAVHD)." *Medical engineering & physics* 18, no. 1 (1996): 26-35.
- [24]. Raj, Dominic SC, Michaelene Ouwendyk, Robert Francoeur, and Andreas Pierratos. " β 2-Microglobulin kinetics in nocturnal haemodialysis." *Nephrology Dialysis Transplantation* 15, no. 1 (2000): 58-64.
- [25]. Legallais, C., Catapano, G., Von Harten, B. and Baurmeister, U., 2000. A theoretical model to predict the in vitro performance of hemodiafilters. *Journal of Membrane Science*, 168(1-2), pp.3-15.
- [26]. Coli, L., M. Ursino, A. De Pascalis, C. Brighenti, V. Dalmastrì, G. La Manna, E. Isola et al. "Evaluation of intradialytic solute and fluid kinetics." *Blood purification* 18, no. 1 (2000): 37-49.
- [27]. Galach, Magda, Anna Ciechanowska, S. Sabalińska, Jacek Waniewski, Jan Wójcicki, and A. Weryńskis. "Impact of convective transport on dialyzer clearance." *Journal of Artificial Organs* 6, no. 1 (2003): 0042-0048.
- [28]. Waniewski J, Werynski A, Ahrenholtz P, Lucjanek P, Judycki W, Esther G. Theoretical basis and experimental verification of the impact of ultrafiltration on dialyzer clearance. *Artif Organs* 1991; 15:70–77
- [29]. Jaffrin, Michel Y., Luhui Ding, and Jean Marc Laurent. "Simultaneous convective and diffusive mass transfers in a hemodialyser." (1990): 212-219.
- [30]. Conrad, S. A., and A. Bidani. "Finite element mathematical model of fluid and solute transport in hemofiltration membranes." In *Proceedings of the 25th Annual International Conference of the IEEE Engineering in Medicine and Biology Society (IEEE Cat. No. 03CH37439)*, vol. 1, pp. 423-426. IEEE, 2003.
- [31]. E. W. Merrill, "Rheology of blood," *Physiol Rev* vol. 49, no. 4, pp. 863-88, 1969.

- [32]. Mimouni, Zineb. "The Rheological Behavior of Human Blood—Comparison of Two Models." *Open Journal of Biophysics* 6, no. 2 (2016): 29-33.
- [33]. Gałach, M., and A. WERY NSKI. "Development of "virtual patient" model for simulation of solute and fluid transport during dialysis." *TECHNICAL SCIENCES* 53, no. 3 (2005).
- [34]. Yamamoto, Ken-ichiro, Masayo Hayama, Masato Matsuda, Taiji Yakushiji, Makoto Fukuda, Takehiro Miyasaka, and Kiyotaka Sakai. "Evaluation of asymmetrical structure dialysis membrane by tortuous capillary pore diffusion model." *Journal of membrane science* 287, no. 1 (2007): 88-93.
- [35]. Azar, Ahmad Taher. "Increasing dialysate flow rate increases dialyzer urea clearance and dialysis efficiency: an in vivo study." *Saudi Journal of kidney diseases and transplantation* 20, no. 6 (2009): 1023.
- [36]. Lu, Junfeng, and Wen-Qiang Lu. "A numerical simulation for mass transfer through the porous membrane of parallel straight channels." *International Journal of Heat and Mass Transfer* 53, no. 11-12 (2010): 2404-2413.
- [37]. Gambro. Polyflux™ H – Gambro. [Online]. Available at: www.gambro.com/PageFiles/7431/HCEN2489_5%20Polyflux_H.pdf?epslanguage=en (Accessed: 29 March 2020)
- [38]. Annan, Kodwo. "Mathematical modeling for hollow fiber dialyzer: Blood and HCO₃–dialysate flow characteristics." *International Journal of Pure and Applied Mathematics* 79, no. 3 (2012): 425-452.
- [39]. Davenport, Andrew. "How can dialyzer designs improve solute clearances for hemodialysis patients?." *Hemodialysis International* 18 (2014): S43-S47.
- [40]. Ding, Weiping, Weili Li, Sijie Sun, Xiaoming Zhou, Peter A. Hardy, Suhail Ahmad, and Dayong Gao. "Three-Dimensional Simulation of Mass Transfer in Artificial Kidneys." *Artificial organs* 39, no. 6 (2015): E79-E89.
- [41]. Zhang, Qinglei, Xiaolong Lu, Juanjuan Liu, and Lihua Zhao. "Preparation and preliminary dialysis performance research of polyvinylidene fluoride hollow fiber membranes." *Membranes* 5, no. 1 (2015): 120-135.
- [42]. Ravagli, Enrico, Elena Grandi, Paolo Rovatti, and Stefano Severi. "Finite-element modeling of time-dependent sodium exchange across the hollow fiber of a hemodialyzer by coupling with a blood pool model." *The International journal of artificial organs* 39, no. 9 (2016): 471-478.
- [43]. Donato, Danilo, Adriana Boschetti-de-Fierro, Carina Zweigart, Michael Kolb, Sunny Eloot, Markus Storr, Bernd Krause, Ken Leypoldt, and Patrick Segers. "Optimization of dialyzer design to maximize solute removal with a two-dimensional transport model." *Journal of Membrane Science* 541 (2017): 519-528.
- [44]. Sangeetha, M. S., A. Kandaswamy, C. LAKSHMI DEEPIKA, AND CV REVANTH. "FINITE ELEMENT ANALYSIS FOR COMPARING THE PERFORMANCE OF STRAIGHT AND

UNDULATED FIBERS IN ALTERING THE FILTERING EFFICIENCY OF HEMODIALYZER MEMBRANES." *Journal of Mechanics in Medicine and Biology* 19, no. 05 (2019): 1850063.

- [45]. <https://www.comsol.com/model/separation-through-dialysis-258>
- [46]. Ouseph, Rosemary, Colin A. Hutchison, and Richard A. Ward. "Differences in solute removal by two high-flux membranes of nominally similar synthetic polymers." *Nephrology Dialysis Transplantation* 23, no. 5 (2008): 1704-1712.
- [47]. Hedayat, A., J. Szpunar, N. A. P. Kumar, R. Peace, H. Elmoselhi, and A. Shoker. "Morphological characterization of the Polyflux 210H hemodialysis filter pores." *International journal of nephrology* 2012 (2012).
- [48]. Bird, R. Byron. "Transport phenomena." *Appl. Mech. Rev.* 55, no. 1 (2002): R1-R4.
- [49]. Eloot, Sunny, Jan Vierendeels, and Pascal Verdonck. "Optimisation of solute transport in dialysers using a three-dimensional finite volume model." *Computer methods in biomechanics and biomedical engineering* 9, no. 6 (2006): 363-370.
- [50]. McCabe, Warren Lee, Julian Cleveland Smith, and Peter Harriott. *Unit operations of chemical engineering*. Vol. 5. New York: McGraw-hill, 1993.
- [51]. Kirsch, Alexander H., Raphael Lyko, Lars-Göran Nilsson, Werner Beck, Michael Amdahl, Petra Lechner, Andreas Schneider, Christoph Wanner, Alexander R. Rosenkranz, and Detlef H. Krieter. "Performance of hemodialysis with novel medium cut-off dialyzers." *Nephrology Dialysis Transplantation* 32, no. 1 (2017): 165-172.
- [52]. Bhimani, Jai P., Rosemary Ouseph, and Richard A. Ward. "Effect of increasing dialysate flow rate on diffusive mass transfer of urea, phosphate and β 2-microglobulin during clinical haemodialysis." *Nephrology Dialysis Transplantation* 25, no. 12 (2010): 3990-3995.